ktu
1922

KAUNO TECHNOLOGIJOS UNIVERSITETAS

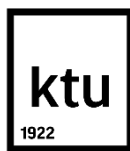**CHEMINĖS TECHNOLOGIJOS FAKULTETAS**

Aleksandras Kolesničenko

DI- IR TETRAHIDRAZONO FRAGMENTUS TURINČIŲ TRIFENILAMINO IR METOKSITRIFENILAMINO DARINIŲ SINTEZĖ IR SAVYBIŲ TYRIMAS

Baigiamasis magistro darbas

Vadovas

doc. dr. Tadas Malinauskas

Kaunas, 2015

ktu
1922

KAUNAS UNIVERSITY OF TECHNOLOGY

FACULTY OF CHEMICAL TECHNOLOGY

Aleksandras Kolesničenko

SYNTHESIS AND INVESTIGATION OF TRIPHENYLAMINE AND METHOXYTRIPHENYLAMINE DERIVATIVES CONTAININGS DI- AND TETRAHYDRAZONE FRAGMENTS

Master's thesis

Supervisor

Asoc. Prof. Dr. Tadas Malinauskas

Kaunas, 2015

KAUNO TECHNOLOGIJOS UNIVERSITETAS

CHEMINĖS TECHNOLOGIJOS FAKULTETAS

ORGANINĖS CHEMIJOS KATEDRA

TVIRTINU

Organinės chemijos katedros vedėjas

Prof. Dr. Vytas Martynaitis

DI- IR TETRAHIDRAZONO FRAGMENTUS TURINČIŲ TRIFENILAMINO IR METOKSITRIFENILAMINO DARINIŲ SINTEZĖ IR SAVYBIŲ TYRIMAS

Baigiamasis magistro darbas

Studijų programa Taikomoji chemija (kodas 612F10003)

Vadovas

Doc. Dr. Tadas Malinauskas

Recenzentas

Dr. Aušra Tomkevičienė

Darbą atliko

Aleksandras Kolesničenko

Kaunas, 2015

KAUNO TECHNOLOGIJOS UNIVERSITETAS

CHEMINĖS TECHNOLOGIJOS FAKULTETAS

Aleksandras Kolesničenko

Studijų programa Taikomoji chemija (kodas 612F10003)

Baigiamojo darbo „ Di- ir tetrahidrazono fragmentus turinčių trifenilamino ir metoksitrifenilamino darinių sintezė ir savybių tyrimas"

AKADEMINIO SĄŽININGUMO DEKLARACIJA

2015 m. _____ mėn. _ _ d.

Kaunas

Patvirtinu, kad mano **Aleksandro Kolesničenko** baigiamasis darbas tema „Di- ir tetrahidrazono fragmentus turinčių trifenilamino ir metoksitrifenilamino darinių sintezė ir savybių tyrimas" yra parašytas visiškai savarankiškai, o visi pateikti duomenys ar tyrimų rezultatai yra teisingi ir gauti sąžiningai. Šiame darbe nei viena darbo dalis nėra plagijuota nuo jokių spausdintinių ar internetinių šaltinių, visos kitų šaltinių tiesioginės ir netiesioginės citatos nurodytos literatūros nuorodose. Įstatymu nenumatytų piniginių sumų už šį darbą niekam nesu mokėjęs.

Aš suprantu, kad išaiškėjus nesąžiningumo faktui, man bus taikomos nuobaudos, remiantis Kauno technologijos universitete galiojančia tvarka.

_____   _____
(studento vardas ir pavardė, įrašyti ranka)   (parašas)

Santrauka

Augant Žemės gyventojų skaičiui ir senkant iškastiniam kurui, energijos paklausą galėtų patenkinti alternatyvūs energijos šaltiniai, pavyzdžiui, saulės spinduliuotė – ji yra lengviausiai prieinamas, labiausiai paplitęs ir praktiškai neišsenkantis energijos šaltinis. Paverčiant tik 0,02% Žemę pasiekiančios spinduliuotes elektra, visiškai būtų galima patenkinti žmonijai reikalingos energijos poreikį. Tokiam energijos kiekio konvertavimui reikalingi kuo efektyvesni ir pigesni saulės elementai. Įprastiniai silicio saulės elementai yra pakankamai našūs, tačiau pasižymi brangia ir sudėtinga gamyba. Pigesni organiniai ir hibridiniai saulės elementai ilgą laiką nusileisdavo efektyvumu, tačiau pastarųjų kelių metų atradimai artimiausiu metu gali leisti jiems nukonkuruoti tradicinius.

Saulės elementai, kaip ir kiti optoelektroniniai prietaisai, sudaromi iš kelių skirtingas funkcijas atliekančių sluoksnių. Kiekvieną sluoksnį sudarantiems medžiagoms keliami tam tikri reikalavimai. Šio darbo tikslas – susintetinti naujus, literatūroje neaprašytus di- ir tetrahidrazonus su trifenilamino centriniu fragmentu. Hidrazonai pasirinkti, nes atitinka visus keliamus reikalavimus: gali sudaryti patvarius amorfinius sluoksnius kambario temperatūroje, turi aukštą krūvininkų judrį, pasižymi tinkamu jonizacijos potencialu kietoje būsenoje.

Siekiant darbe užsibrėžto tikslo, atliktos daugiapakopės sintezės, nereikalaujančios brangių reagentų ar katalitinių sistemų, ir susintetinti šie junginiai:
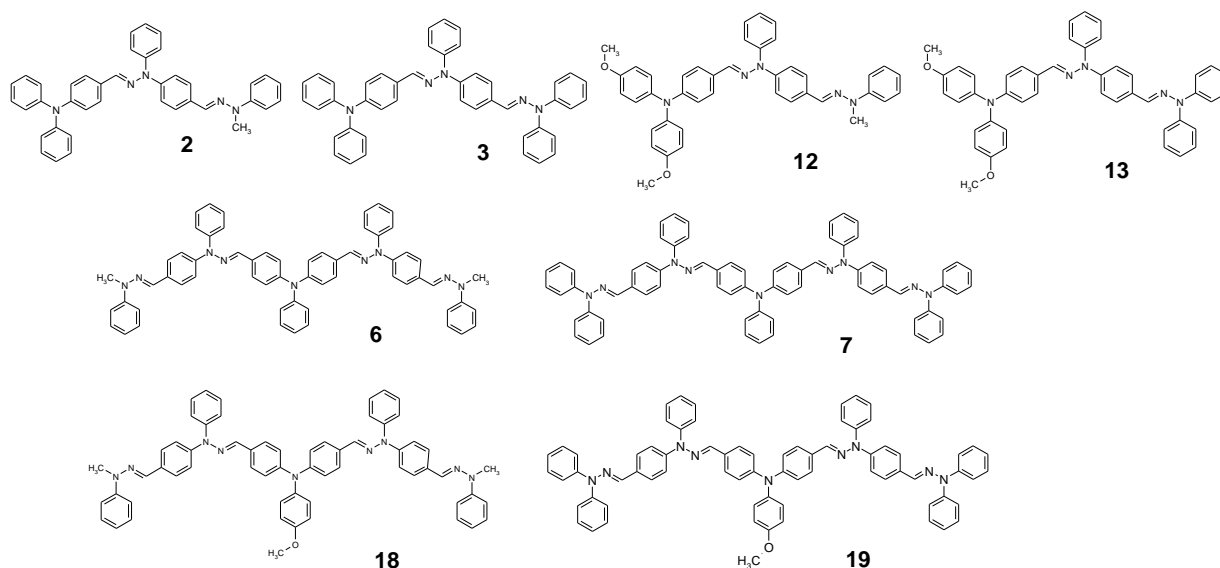
Ištirtos terminės, optoelektrinės ir elektrocheminės susintetintų junginių savybės. Taip pat išmatuoti saulės elementų, pagamintų naudojant susintetintus junginius, darbiniai parametrai (lentelė 1, 2).

Lentelė 1. Terminės, optoelektrinės bei elektrocheminės susintetintų junginių savybės.

Junginys	T_g, C°	T_m, C°	λ_A, nm	μ^a, cm^{2}V^{-1}s^{-1}	E_{ox}, V vs NHE	I_p, eV
2	42	182	392	$2,9\times10^{-4}$	0.97	5,26
3	89	129	395	$5,6\times10^{-4}$	0.80	5,22
6	95	-	406	$3,6\times10^{-5}$	0.93	5,17
7	100	-	397	$3,6\times10^{-5}$	0.85	5,17
12	45	142	396	$4,7\times10^{-5}$	0,74	5,16
13	69	182	400	$4,6\times10^{-5}$	0,77	5,22
18	105	-	415	$2,5\times10^{-3}$	0.77	5,15
19	85	-	409	$2,4\times10^{-3}$	0.76	5,10

a – pateiktos dreifinio judrio reikšmės (μ) nustatytos esant elektros lauko stiprumui $E = 6,4 \times 10^5$ Vcm^{-1}

Lentelė 2. Saulės elementų sudarytų naudojant susintetintus junginius darbiniai parametrai

Junginys	saulės elemento tipas	J_{sc}, mA cm^{-2}	V_{oc}, V	FF, %	η, %
2	ssDSSC	2,38	0,54	34	0,4
3	ssDSSC	2,52	0,66	40	0,7
6	ssDSSC	1,64	0,64	30	0,3
7	ssDSSC	1,78	0,6	33	0,3
12	ssDSSC	0,69	0,52	46	0,2
13	ssDSSC	3,35	0,82	36	1
18	ssDSSC	5,59	0,68	42	1,6
12	PSC	6,19	0,46	35	1
18	PSC	4,83	0,84	26	1,1

Išanalizavus gautus duomenis buvo padarytos išvados, kad nors susintetintų junginių terminės, optoelektrinės ir elektrocheminės savybės teoriškai leistų juos panaudoti našių saulės elementų konstravimui, bandymų metu aukštų našumų gauti nepavyko. Galima daryti prielaidą, kad tai lėmė prastas susintetintų puslaidininkių suderinamumas su prietaisų konstravimo metu naudojamais oksiduojančiais priedais.

Summary

An ever increasing Earth's population and dwindling conventional resources create a demand for alternative, renewable energy producing technology. The Sun provides an immense supply of energy which if correctly harvested could completely satisfy humanity's need for energy. Recent developments in the field of organic-inorganic hybrid solar cells might allow them to replace the more expensive, yet still more efficient inorganic solar cells.

Solar cells, like many other optoelectronic devices consist of several functional layers. To further their progress, there is a constant search for new materials for the fabrication of said layers. This work focuses on hole transporting materials for solar cells. New, di- and tetrahydrazones with a triphenylamine based core fragment have been synthesized as part of this work. Hydrazones were chosen because they meet the requirements for such a class of materials: they are able to form stable amorphous films, demonstrate good charge drift mobilities and can possess compatible ionization potentials.

The thermal, optoelectric and electrochemical properties of the synthesized materials have been investigated. With glass transition temperatures up to 105 °C, hole drift mobilities as high as 2.5×10^{-3} cm^{2}V^{-1}s^{-1} and ionization potentials as low as 5.1 eV, the synthesized materials should be able to act as efficient hole transporting materials for solid-state solar cells. During preliminary solar cell tests the hydrazones demonstrated power conversion efficiencies as high as 1.6% in solid state dye-sensitized solar cells and 1.1% in perovskite solar cells.

Judging from the testing results the doping procedures used for spiro-MeOTAD are not that suitable for these materials. Most likely higher ionization potential of the investigated hydrazones hampers the doping process and the conductivity remains low, which is evident from rather low fill factor. Further optimization of the doping procedure and device construction is necessary in order to enhance the performance of these hole transporting materials in solar cells.

List of abbreviations

α	*Poole-Frenkel* parameter;
ε	extinction coefficient;
δ	chemical shifts parameter;
λ	wavelength;
η	solar energy to electricity conversion efficiency;
μ_0	zero field charge carrier mobility;
μ	charge carrier mobility;
ν	wavelength in cm^{-1};
^{1}H NMR	proton nuclear magnetic resonance;
^{13}C NMR	carbon nuclear magnetic resonance;
Acetone-d6	deuterated acetone
$CDCl_3$	deuterated chloroform
CV	cyclic voltammetry;
d	layer thickness;
d	doublet
DMF	dimethylformamide
DSC	differential scanning calorimetry;
DSSC	dye sensitized solar cell;
E	electric field;
Fc	ferrocene;
FF	fill factor;
FTO	fluorine-doped tin oxide;
HOMO	highest occupied molecular orbital;
HTM	hole transporting material;
I_p	ionization potential;
ITO	indium tin oxide;
J	coupling constant in Hz;
*J*sc	short circuit current;
LiTFSI	Lithium trifluoromethane sulfonimide
NaO(t-Bu)	sodium tert-butoxide
m	multiplet
PCE	power conversion efficiency;
Pd_2dba_3	tris(dibenzylideneacetone)dipalladium (0)
$Pd(OAc)_2$	palladium acetate (II)
$P(t-Bu)_3$	tri-tert-butylphosphine
ppm	parts per million;
s	singlet
spiro-MeOTAD	2,2',7,7'-tetrakis-(*N*,*N*-di-*p*-methoxyphenylamine)-9,9'-spirobifluorene;
ssDSSC	solid-state dye-sensitized solar cell;
t	triplet
T	temperature;
T_g	glass transition temperatures;
T_m	melting point;
THF	tetrahydrofurane
TLC	thin layer chromatography;
TMS	trimethylsilane;
TPA	triphenylamine;
UV-Vis	ultraviolet/visible;
V_{oc}	open circuit photovoltage;
XTOF	xerographic time of flight technique.

Contents

1. Introduction

The continuous exponential growth of Earth's population creates an insurmountable need for energy. As conventional energy resources such as fossil fuel gradually dwindle, humanity's gaze is ever turned towards a sustainable sociotechnological model the main pillars of which are - recycling, power saving technologies and renewable energy.

Out of all available alternative energy sources, solar energy is the most abundant and ubiquitous. Converting 0.02% of the Sun's irradiation that reaches the Earth's surface would completely satisfy the populaces demand for energy [1]. Inorganic photovoltaic devices are rather efficient and long-lasting yet their production includes complicated and costly technological processes. Organic and hybrid solar cells are less efficient, but a wide variety of available functional materials and relatively inexpensive production makes them an attractive choice, especially in light recent developments in the area of solid state hybrid photovoltaics.

As with every significant new technology there's a surge in demand for new materials. Specifically there's a need for new, effective p-type semiconductors which meet a number of requirements including, but not limited to: the ability to form stable amorphous layers, high charge drift mobility, and compatible energy levels. Aryl hydrazones are a convenient choice since they're relatively inexpensive and usually meet most of the aforementioned requirements [2].

The main aim of this work:

synthesize di- and tetrahydrazones with triphenylamine (TPA) based core fragments applicable as hole transporting materials in photovoltaic devices.

Tasks proposed to achieve the aim:

- synthesis of di- and tetrahydrazones with TPA based cores
- investigation of thermal, photoelectric and electrochemical properties of the synthesized materials and exploring the influence of molecular structure on said properties
- testing the synthesized materials in solid-state solar cells.

2. Literature review

As stated above the main goal of this work is the creation and study of organic molecular HTMs for photovoltaic devices. For such a purpose it would be prudent to first study the said devices, then present an overview of the qualities the created materials should posses as well as a review of organic molecular HTMs already reported in scientific literature. Accordingly, this literary review provides a general description of the composition and functioning principle of two prominent types of photovoltaic devices – dye-sensitized solar cells and perovskite solar cells; further an analysis of the characteristics used to evaluate the HTMs and their relation to chemical structure is related and finally a short review of several categories of reported HTMs.

2.1 Dye-sensitized solar cells
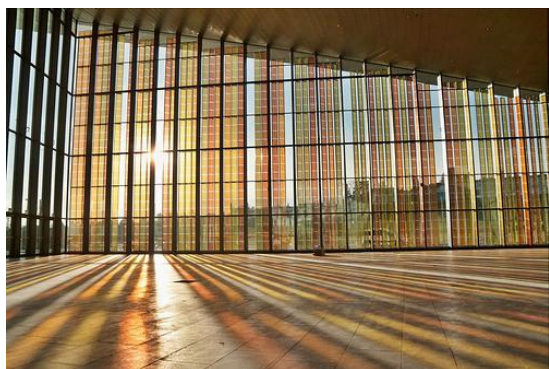
Picture 2-1. Colored, semitransparent DSSCs used as a functional decorative material in a convention canter in Lausanne, Switzerland

Dye-sensitized solar cells (DSSC) with power conversion efficiency (PCE) of over 7% were first reported in 1991 by M. Grätzel and since then have seen many years of steady development. Even though these devices cannot trump the monocrystaline silicon based solar cells in efficiency they possess a number of considerable advantages. DSSCs are easy to fabricate with a wide choice of relatively inexpensive functional materials, they can also be manufactured as colored and semi-transparent modules of various shapes which allows incorporating them into many architectural and industrial designs.

Figure **2-1 A** demonstrates the general configuration of a DSSC device. From bottom to top the device parts are as follows: a partially etched conducting glass substrate – fluorine-doped tin oxide (FTO), alternatively indium-doped tin oxide ITO can be used; a thin, dense TiO_2 film which prevents short circuits between the transparent conductive oxide (TCO) substrate and the HTM layer; a layer of mesoporous TiO_2 (spherical anatase) sensitized by photon absorbing dye molecules; a HTM layer which in classical DSSCs consists of a liquid electrolyte (usually $I_3^-/3I^-$) and a solid-state molecular or polymeric semiconductor in solid-state dye-sensitized solar cells (ssDSSC); and a counter electrode (Au, Ag).
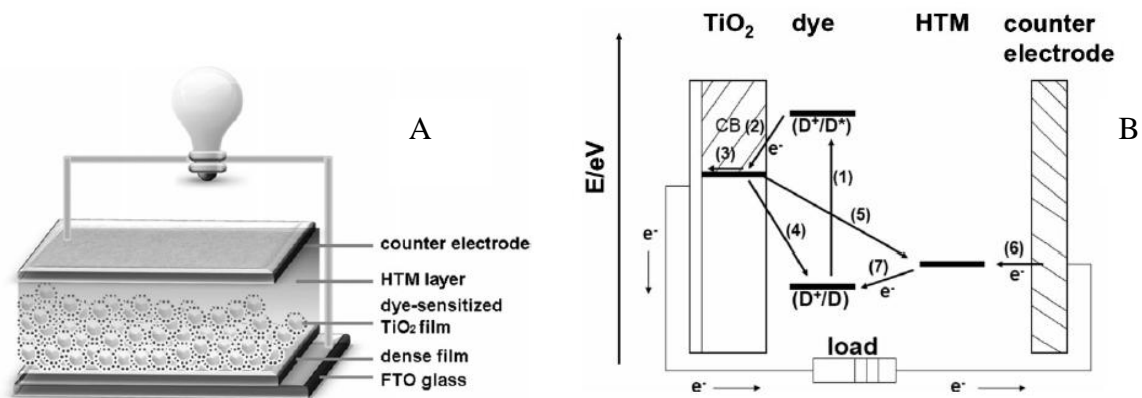
Figure 2-1. A – the layout of functional materials within a dye-sensitized solar cell; B – electron movements within a dye-sensitized solar cell.

Figure **2-1 B** shows the basic operation principle of a DSSC. When a dye-sensitizer molecule absorbs a photon of light it enters an excited state (process 1) upon which, an electron is injection into the conduction band of TiO_2 (process 2). The oxidized dye is later regenerated by the electron injection from the HTM (process 7). The electrons from the TiO_2 conduction band and the holes from the HTM, are subsequently collected by the FTO substrate (process 3) and the counter electrode (process 6) accordingly thus closing an electric circuit. Some undesirable processes may occur alongside the main cycle. For example electrons from the TiO_2 conduction band can recombine with the oxidized dye molecules (process 4) and the HTM (process 5) [3].
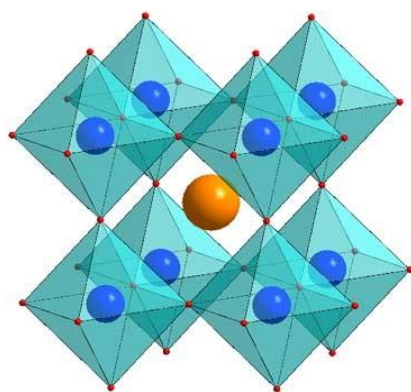
2.2 Perovskite solar cells

Figure 2-2. Crystal lattice structure of cubical perovskite with the general forumal ABX_3

An important step in the development of DSSC technology was the discovery of perovskite light absorbers. Perovskites refer to a class of materials with the general formula ABX_3 where X is an anion, A and B are cations of different size (A being bigger than B). In an ideal case perovskites form a specific cubical structure as shown in figure **2-2**. The most commonly used perovskites have $CH_3NH_3^+$ as cation A, lead (II) or tin (II) as cation B and halides with an exception of fluorine as the anion X. Even though the first attempt to incorporate perovskites into DSSC devices as the sensitizing dye was undertaken in 2009 it met no great success as the perovskites would quickly degrade under the aggressive effect of the liquid electrolyte. In 2012 Snaith et al. and Grätzel et al. independently developed solid state DSSC using $CH_3NH_3PbI_3$ as the absorber and spiro-MeOTAD as the HTM

3

with PCEs of 7.6% and 9.7% respectively[4, 5]. Since then perovskite solar cells (PSCs) have enjoyed constant and rapid development.

Essentially PSC composition and principle of functioning is the same as for other ssDSSCs with slight differences. For example perovskites can act both as an absorber and electron transfer layer allowing changing the mesoporous TiO_2 scaffold with a significantly cheaper Al_2O_3. A primary shortcoming of PSCs is poor longevity in humid conditions since water leads to a rapid degradation of the perovskite.

2.3 Hole transport material characteristics and parameters

It is required that solid state HTMs would form stable amorphous glass layers. Opposite to crystalline, amorphous layers don't have grain boundaries which means they are homogenous in their properties, suffer less charge loss and are mechanically tough yet flexible. An amorphous state also solves the problem of filling in the pores of a sensitized scaffold within solid-state solar cells leading to improved charge injection and subsequently more efficient overall device performance [6]. Hence the importance of morphological stability, guaranteeing that devices will maintain functionality in harsh conditions.

Qualities mentioned above can be quantified by the material's glass transition temperature (T_g). Even though many organic molecules readily form crystals below melting temperature (T_m) it has been observed that materials with higher T_g values and certain structural nuances are more likely to form amorphous layers when rapidly cooled as well as maintaining them for longer periods of time. Such tendencies were described by H. O. Wirth [7]:

- larger and more rigid molecular structures lead to higher T_g values
- symmetrical molecules are more likely to form crystals thus a certain degree of structural disorder is necessary
- introducing long flexible aliphatic moieties improves morphological stability and decreases brittleness of the layer.

Fast charge transport is essential for an efficient semiconductor. This quality is described by charge drift mobility (μ). Charge drift mobility (in the case of HTMs – hole drift mobility) is defined as the distance a single charge travels pulled by an electrical field which magnitude (E) equals 1, per unit of time. The charge drift mobility is influenced by temperature (T), external electrical field (E), pressure (P) and the structure of the semiconductor [8].

The most orderly solid-state systems – monocrystals have highest charge drift mobility, unfortunately their manufacture is complicated and costly process and the resulting crystals are rather brittle. Amorphous glasses usually display values lower by several orders of magnitude

and even within amorphous layers, materials with more rigid and orderly molecular structure display higher μ values [9]. However it has been demonstrated that very orderly molecular structures are not optimal when applied as HTMs for solid-state solar cells [10].

Another important parameter is the solid state ionization potential (I_p). It is defined by the minimum amount of work necessary to remove an electron from a molecule's highest occupied molecular orbital (HOMO) [11]. In order to ensure that charge travels through optoelectronic devices without loss, the ionization potentials of each functional layer must be within certain limits.

Since the end goal of this work was to test new molecular structures as HTMs in solar cells, the fabricated devices have to be characterized by the following parameters:

- the V_{oc} is the difference in electrical potential between two terminals of a cell under illumination when the circuit is open (no current flow)
- short-circuit current density J_{sc} is the photocurrent per unit area (mA cm^{-2}) when the voltage across the solar cell under irradiation is zero (i.e., when the solar cell is short circuited)
- the fill factor (FF) is a parameter which, in conjunction with V_{oc} and J_{sc}, determines the maximum power output of a solar cell
- power conversion efficiency (PCE) or η is defined as the ratio of energy output from the solar cell to input energy from the sun [12].

Solar cell characterization is conventionally carried out under standard testing conditions described by a temperature of 25°C, an irradiance of 1000 W/m^2 and 1.5 air mass spectrum.

2.4 Structures reported as hole transporting materials in solid state solar cells

Hole transport in solar cells can be carried out by a wide array of substances and systems – inorganic electrolytes, organic molecules, organometallic complexes, inorganic salts, organic polymers, liquid crystals etc. Since this work focuses on creation of organic molecular structures, this literature review focuses mainly on the already reported substances of this class and its closest "relatives" – organic polymers.

2.4.1 Hole transporting materials with *N,N*-di-*p*-methoxyphenylamine moieties

In 1998 the first ssDSSC was created using 2,2',7,7'-tetrakis(*N,N*-di-*p*-methoxyphenylamine)-9,9'-spirobifluorene (spiro-MeOTAD). It demonstrated an overall efficiency of 0.74% [13]. The efficiency of the first fully solid-state PSC in which spiro-MeOTAD was used as an HTM was 10% [4, 5]. Since then through many optimizations spiro-MeOTAD has become the benchmark HTM for both ssDSSCs and PSCs. A good demonstration

of its potential is that throughout the years the efficiency of PSCs with spiro-MeOTAD has grown to 19% through meticulous modifications of the absorber layer alone [14, 15, 16].

A number of attempts to modify and improve spiro-MeOTAD have been undertaken by various researchers. One of the approaches is focus on the position of the methoxy moieties. From a chemical perspective the methoxy groups were introduced into spiro-MeOTAD in order to control the oxidation potential of the material. The methoxy group is electron-withdrawing by the inductive effect, but it can also exhibit electron-donating behaviour under resonance stabilization. Two opposite effects of the methoxy substituent have been reported. Depending on the substitution position in the aromatic ring: electron-donating at the para position and electron-withdrawing at the meta position. In addition to such electronic effects, substitution at the ortho position can also influence the oxidation potential by steric effects. Therefore it was attempted to fine-tune the electronic properties by changing the substitution position of the methoxy moieties within spiro-MeOTAD (scheme **2-1**) [17].
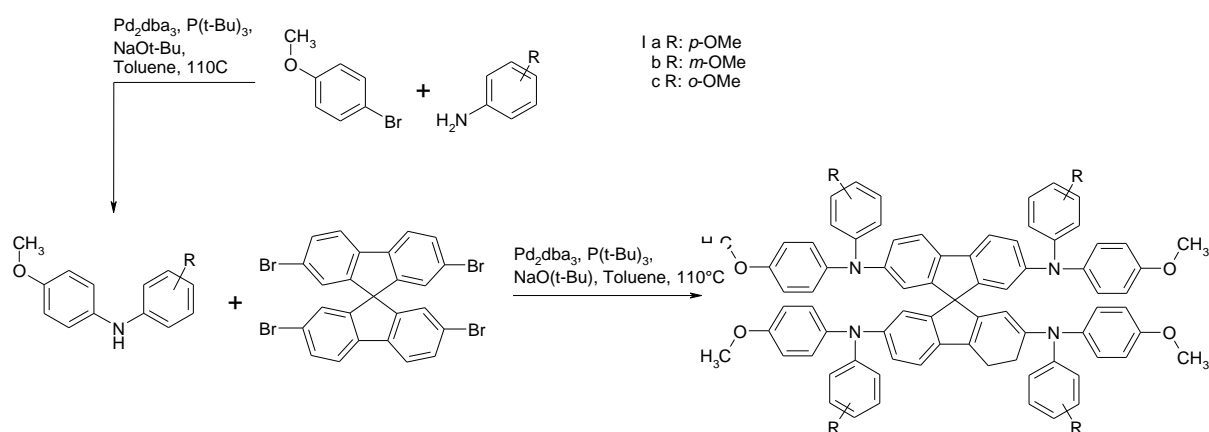
Scheme 2-1. Synthesis of spiro-MeOTAD derivatives

Table 2-1. Solar cell characteristics utilizing spiro-MeOTAD with methoxy substituents in different positions.

Structure	J_{sc}, mA cm^{-2}	V_{oc}, V	*FF*, %	η, %
I a	20.7	1.00	71.1	14.9
I b	21.1	1.01	65.2	13.9
I c	21.2	1.02	77.6	16.7

As it can be seen in table **2-1**, tests demonstrate that the device with ortho substituted spiro-MeOTAD displayed the highest overall efficiency which was attributed to the higher fill factor provided by structure **I c**. This is a good example of how small changes in molecular structure and special arrangement can substantially influence the crucial parameters.

Another common technique to improve charge transport and conductivity of spiro-MeOTAD (as well as that of other *p*-type semiconductors) is chemical doping using p-dopant salts, protic ionic liquids [18, 19] or synthesizing predoped HTMs [20]. Some of dopants used

for improving HTM performance are presented in figure **2-3**. However it has been noticed that the use of dopants lessens the stability of PSC devices. This was attributed to the hydroscopic nature of most additives and their gradual decomposition and subsequential migration of nonfunctional impurities through the HTM layer [21, 22, 23]. It should be considered that all the HTMs presented further in this literature review have been used in conjunction with p-dopants (most often LiTFSI), if not mentioned otherwise.
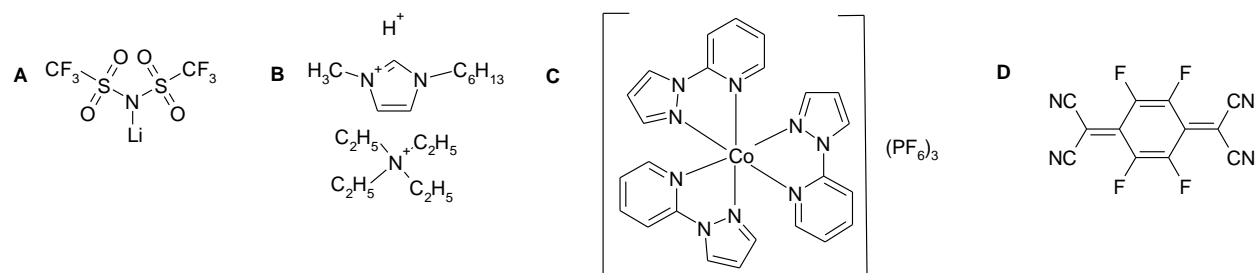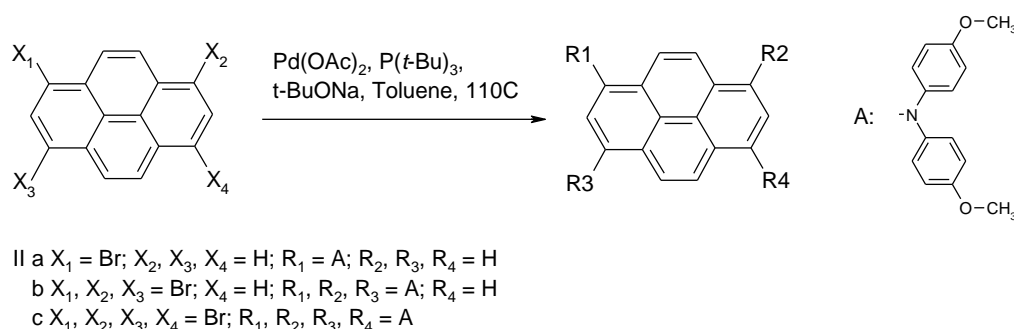

Figure 2-3. Representatives of various p-dopant types used in conjunction with HTMs. A – Lithium trifluoromethane sulfonimide; B – cations used in protic ionic liquids with a TFSI⁻ anion; C – FK109 Cobalt (III) complex; D – tetrafluoro tetracyanoquinodimethane

Even though spiro-MeOTAD remains the benchmark of HTM in ssDSSCs and PSCs, there is much room for improvement. For one, its multistage synthesis using palladium catalysts is rather expensive. A cheaper version of an HTM with *N,N*-di-*p*-methoxyphenylamine moieties has been reported. It's built around a pyrene central fragment, the synthesis is presented in scheme **2-2** and solar cell characterization parameters in table 2 [24].

II a X_1 = Br; X_2, X_3, X_4 = H; R_1 = A; R_2, R_3, R_4 = H
  b X_1, X_2, X_3 = Br; X_4 = H; R_1, R_2, R_3 = A; R_4 = H
  c X_1, X_2, X_3, X_4 = Br; R_1, R_2, R_3, R_4 = A

Scheme 2-2. Synthesis of HTMs with a pyrene core.

Table 2-2. Solar cell, utilizing pyrene based HTMs, characterization properties.

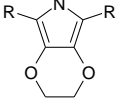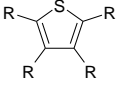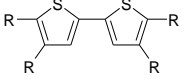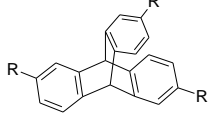| Structure	HOMO, eV	J_{sc}, mA cm^{-2}	V_{oc}, V	*FF*, %	η, %
II a	-5.41	10.8	0.89	35	3.3
II b	-5.25	20.4	0.95	64	12.3
II c	-5.11	20.2	0.89	69	12.4

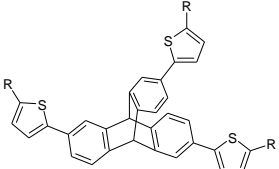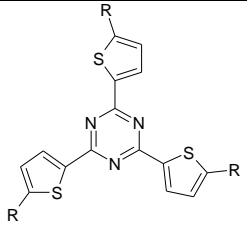The weaker performance of compound **IIa** could be attributed to it's deeper HOMO value thus giving it an insufficient driving force for hole injection.
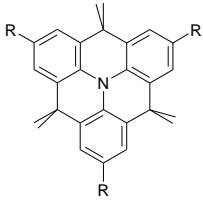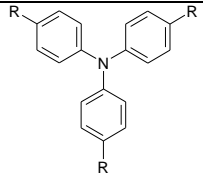
2.4.2 Hole transporting materials with *p*-dimethoxy substituted triphenylamine moieties

This group of materials envelopes *p*-dimethoxy substituted triphenylamine based derivatives with various central fragments. The central core fragments and the solar cell characterization parameters are presented in table **2-3**. As it can be seen, most of these structures demonstrate reasonably high efficiencies, but not higher than spiro-MeOTAD, however the initial materials for most of these are cheaper than those for spiro-MeOTAD [25, 26, 27, 28, 29].

Table 2-3. Structures and solar cell characteristics of dimethoxy triphenylamine based HTMs.

*Structure	HOMO, eV	J_{sc}, mA cm^{-2}	V_{oc}, V	*FF*, %	η, %
III a	-5.16	20.5	1.04	65	13.8
III b	-5.31	19.8	1.08	72	15.4
III c	-5.29	20	1.07	71	15.2
III d	-5.35	17.2	1.03	69	12.2
III e	-5.33	20.3	0.99	62	12.4
III f	-5.04	20.7	0.92	66	12.5

*Structure	HOMO, eV	J_{sc}, mA cm^{-2}	V_{oc}, V	FF, %	η, %
III g	-5.15	21.0	0.97	67	13.6
III h	-5.13	20.9	0.95	62	12.3

* R = *N,N*-bis(4-methoxyphenyl)aniline

2.4.3 Carbazole based hole transporting materials

Another relative structural group of hole transporting semiconductors are *N,N*-di-*p*-methoxyphenylamine disubstituted carbazole derivatives. This group of materials is based on the same principle as the previous groups – creating structures consisting of several methoxy substituted aromatic fragments with conjugated π-electron systems. In the case of carbazole based derivatives such an approach yielded some good results with substances **IV a** and **IV b** demonstrating efficiency on par with spiro-MeOTAD (14.8% and 13.9% respectively) [30].
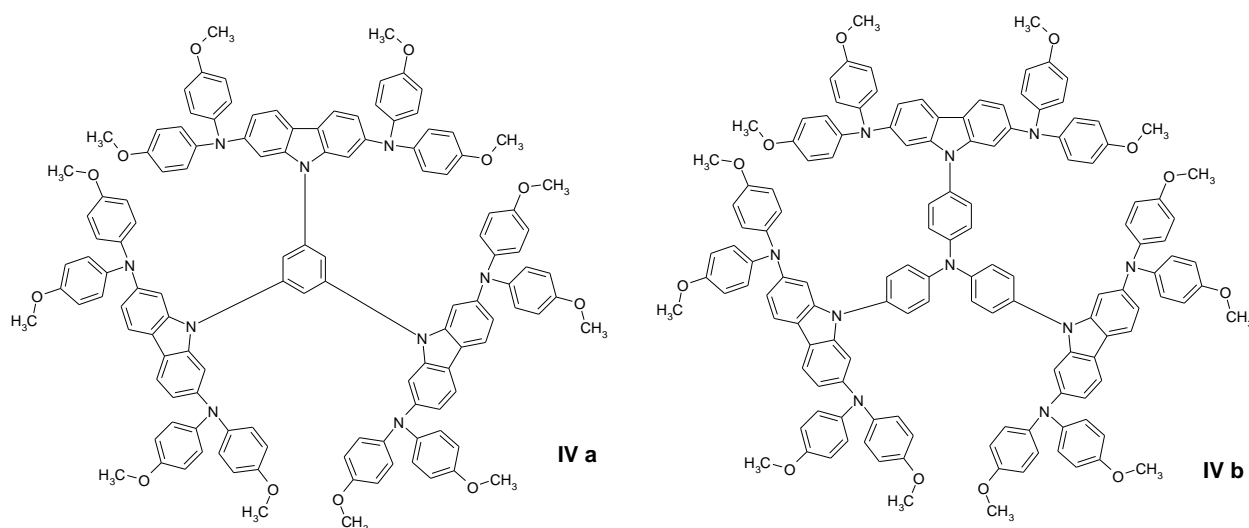

Figure 2-4. *N,N*-di-*p*-methoxyphenylamine disubstituted carbazole derivatives **IV a**, **IV b**.

9

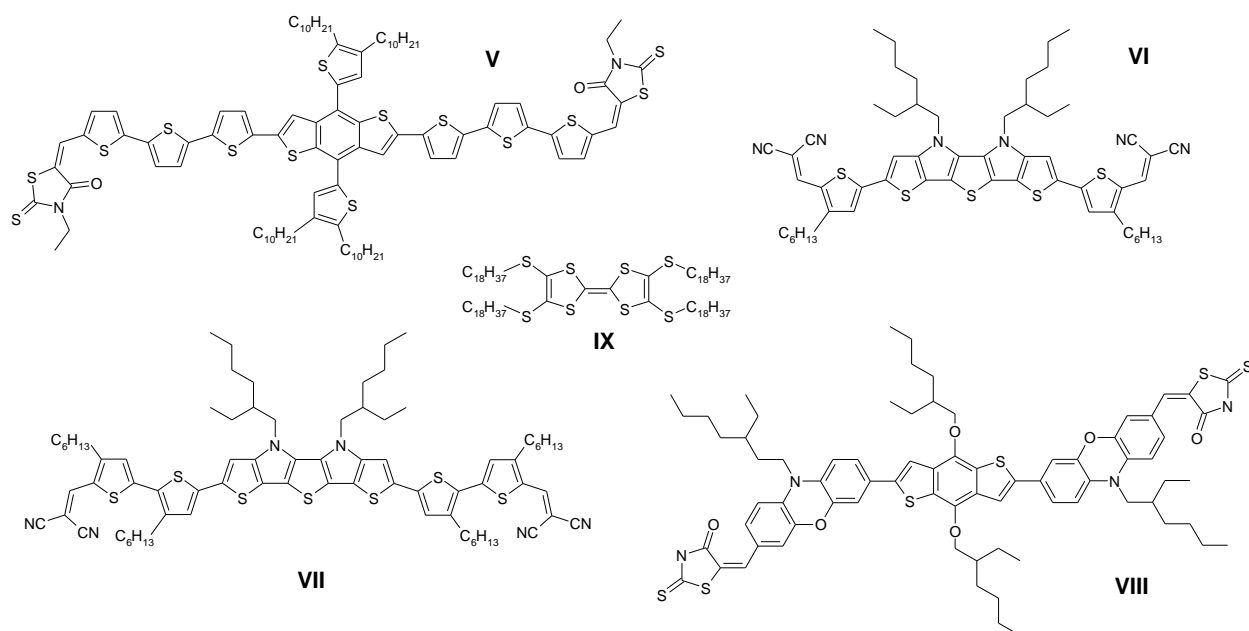## 2.4.4 Heterocycle based hole transporting materials

Figure 2-5. Structures of heterocycle based hole transporting materials **V-IX**.

Some of the most interesting qualities among organic molecular HTMs belong to heterocyclic structures shown in figure **2-5**. These substances demonstrate worthy PCE in pristine condition when used in PSCs (table **2-4**). Some of them demonstrate that p-dopants cause perovskite degradation. For example the oligotiophene based on a benzoditiophene central core (**V**) shows a much higher stability.

Table 2-4. Solar cell characteristics of heterocycle based HTMs.

Structure	HOMO, eV	J_{sc}, mA cm^{-2}	V_{oc}, V	*FF*, %	η, %
V	-5.39	15.3	0.95	60	8.8
VI	-5.26	16.4	0.99	65	10.5
VII	-5.10	15.2	0.9	69	9.5
VIII	-5.29	19.1	1.02	68	13.2
IX	-5.05	19.9	0.86	64	11

The researchers, who reported this material, attribute it to its high water contact angle meaning the material is strongly hydrophobic. When used in conjunction with LiTFSI, the water contact angle and the stability of the device with HTM **V** reduced significantly, indicating the undesirable hydroscopic quality of dopant salt [21]. Another HTM which demonstrates high stability and efficiency on par with doped spiro-MeOTAD, when used pristine is a tetrathiafulvalene derivative **IX** [22]. Other oligotiophene based HTMs **VI** and **VII** were reported to contribute to light absorption in the longer wavelength area of the spectrum forming a dual light-harvesting system together with the perovskite layer [31].
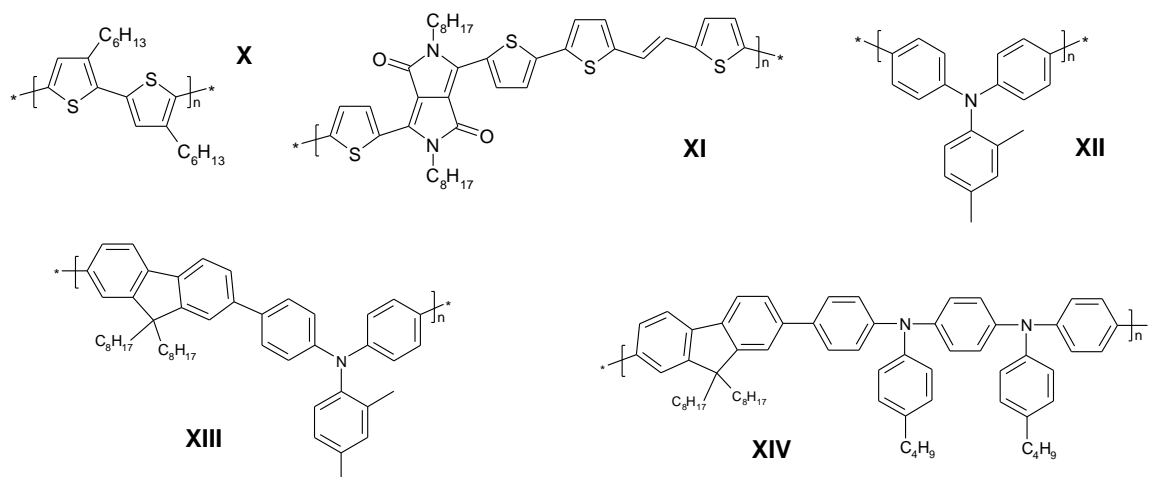
2.4.5 Polymeric hole transport materials

Figure 2-6. Structures of prominent polymeric HTMs **X**-**XIV**.

Polymers make up a large group of HTMs, in this review only some of the more efficient or otherwise noteworthy specimens are presented. Poly(3-hexyltiophene-2,5-diyl) (**X**) is the most studied and most used conducting polymer. Though it demonstrates a reasonably high PCE it also demonstrates a very high hole-electron recombination rate. This was explained by the flat molecular structure coming into very close contact with the sensitizer. This demonstrates why HTM structures should not be entirely flat [32, 33]. Another interesting material is tiophene based polymer **XI**, similar to the oligotiophene **V** it demonstrates greatly increased stability in humid conditions due to its hydrophobic properties [34]. The dimethyl substituted polytriarylamine **XII** is reported to have some sort of chemical interaction with perovskites which allows for very high efficiencies [35], however attempts to expand on the success by creating various polymeric triarylamine based derivatives haven't seen much success so far [36, 37]. The results of the characterization of solar cells fabricated with use of the polymers described above are presented in table **2-5**.

Table 2-5. Solar cell characteristics of polymeric HTMs.

Structure	HOMO, eV	J_{sc}, mA cm^{-2}	V_{oc}, V	FF, %	η, %
X	-5.20	20.8	0.92	54	10.4
XI	-5.40	14.4	0.86	75	9.2
XII	-5.20	19.5	1.09	76	18.4
XIII	-5.44	6.3	1.36	70	6
XIV	-5.10	13.8	0.91	64	8

2.4.6 Aryl hydrazones

All the groups of organic molecular HTMs presented above have common shortcoming – complicated synthetic paths which require expensive reagents, palladium catalysts and have to be

carried out in anhydrous solvents and under inert atmospheres. Aryl hydrazones, however can be synthesized in a simple two step procedure: formylation of an aromatic compound followed by a condensation of the yielded aldehyde with a mono- or disubstituted hydrazine (scheme **2-3**). Most often such reactions do not require any special conditions and are catalyzed by acetic acid or its salts [38].

R, R', R" = H, aryl, alkyl
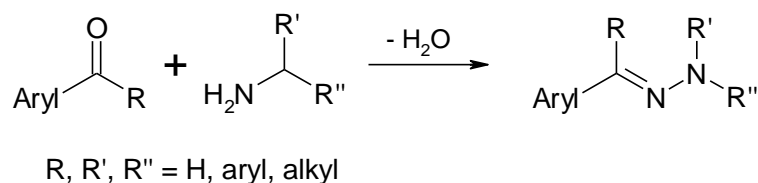
Scheme 2-3. General scheme of aryl hydrazone synthesis.

Aryl hydrazones are a well known class of organic molecular HTMs overall however there are very few reports of them being utilized as HTMs for solar cells and don't show high results [39]. This could be attributed to the fact that only rather small hydrazone based structures were tested. Smaller aryl hydrazones have a tendency for crystallization and usually have deeper HOMO values even though they can still posses high drift mobilities [2]. Both issues can be remedied by creating larger structures with a higher amount of hydrazone moieties. The dendrimeric aryl hydrazone **XV** in figure **2-7** is a good example, with a T_g of 164 C° it demonstrates exceptional morphological stability. I_p values can also be lowered by additional hydrazone moieties due to their electron-donoric properties.
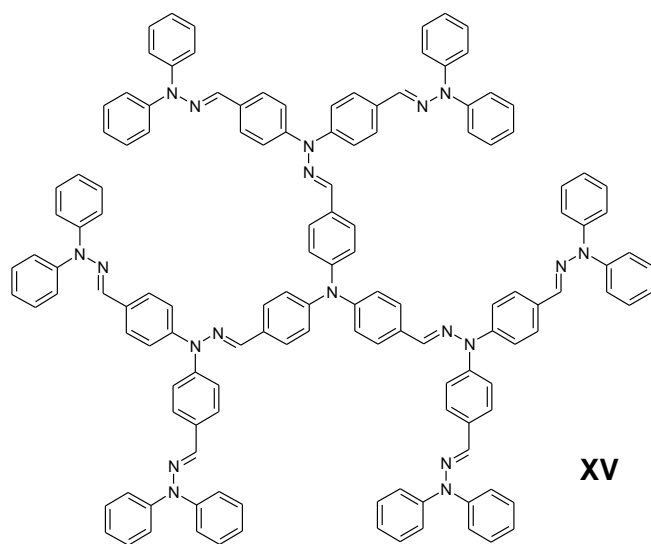

Figure 2-7. Dendrimeric aryl hydrazone **XV**.

2.5 Literature review conclusions

Upon having studied a number of literature a number of conclusions have been made. Effective HTMs for solid state solar cells for the most part resemble spiro-MeOTAD in structure – they all posses a nonplanar spacial structure. Another important feature is the possibility for

optimization by introduction of methoxy moieties which allow the use of performance enhancing dopants. Triphenyalamine based HTMs demonstrate similar qualities, but present a cheaper central fragment, whereas hydrazone moieties can further increase the space occupied by the molecule and could be used to regulate I_p values of structures. All of the aforementioned conclusions lead to the decision to synthesize di- and tetrahydrazones with TPA and methoxy-TPA central fragments.

3. Results and discussion

As human civilization finds itself in an ever increasing need for energy, research of energy saving technologies and devices which convert clean, alternative sources of energy into electricity is highly prioritized. Even though such research is spearheaded by physicists, chemistry is also of paramount importance since chemical synthesis is still a significantly cheaper way to discover and produce multitudes of new materials of various functionality. Good examples are aryl hydrazones which can be easily modified to suite different purposes and are relatively inexpensive to manufacture.

As mentioned in the introduction, this work is a direct continuation of the bachelor thesis. Its goal is exploration of the applicability of aryl hydrazones with a different number of hydrazone moieties as HTMs in organic and hybrid solar cells as well as development of new structures optimized specifically for such application. This part of the work focuses on the synthesis of said aryl hydrazones (specifically triphenylamine di- and tetrahydrazones), investigation of their thermal, optical and photoelectric properties and attempts to explain the relation between molecular structures and the presented properties.
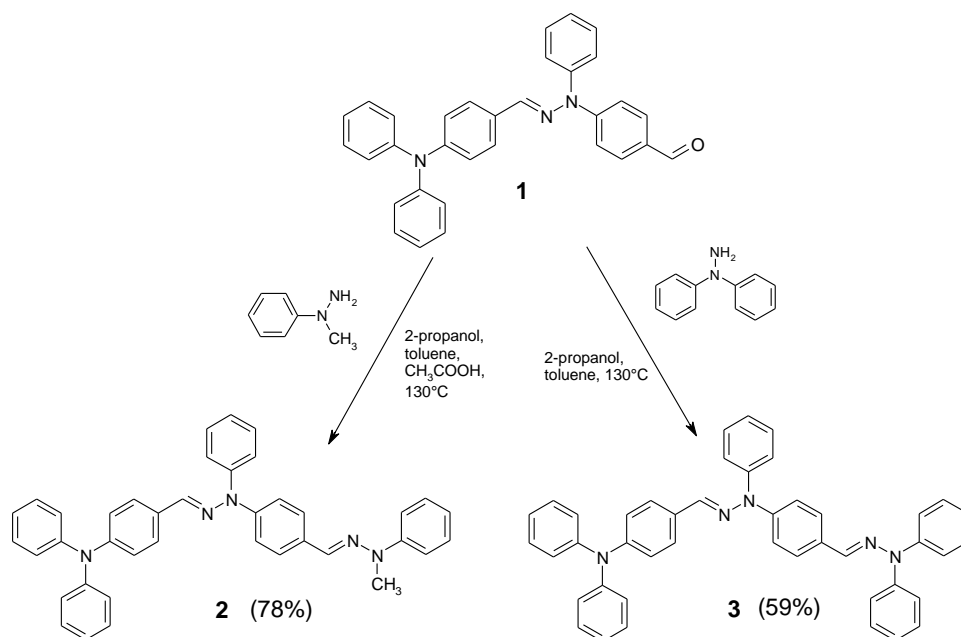
3.1 Synthesis

In order to synthesize the aforementioned hydrazones a multistage synthesis was performed. In the first step 4-{2-[4-(diphenylamino)benzylidene]-1-phenylhydrazinyl}benzaldehyde (**1**) was synthesized from *p*-fluorobenzaldehyde and 4-(diphenylamino)benzaldehyde diphenylhydrazone in anhydrous DMF under argon atmosphere in the presence of base K_2CO_3 as shown in scheme **3-1**.
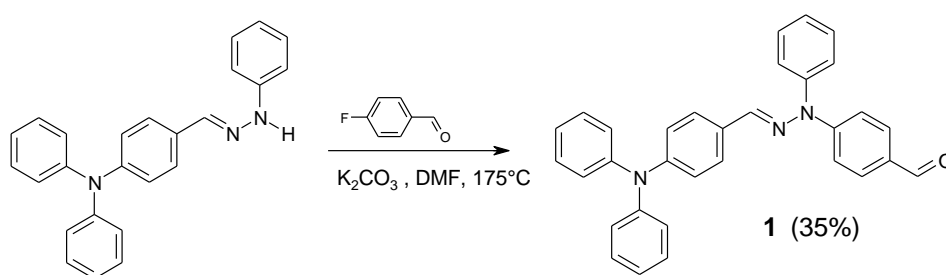
Scheme 3-1. Synthesis of 4-{2-[4-(diphenylamino)benzylidene]-1-phenylhydrazinyl}benzaldehyde (**1**).

Aldehyde **1** was used in the condensation reactions with 1-phenyl-1-methylhydrazine and 1,1-diphenylhydrazine to afford 4-[(2-{4-[(2-methyl-2-phenylhydrazinylidene)methyl]phenyl}-2-phenylhydrazinylidene)methyl]-*N*,*N*-diphenylaniline (**2**) and 4-[(2-{4-[(diphenylhydrazinylidene)methyl]phenyl}-2-phenylhydrazinylidene)methyl]-*N*,*N*-diphenylaniline (**3**) accordingly (scheme **3-2**). The former reaction was carried out in a (2:1 v/v)

solution of toluene and 2-propanol with a catalytic amount of acetic acid; the later − in a (1:1 v/v) solution of toluene and 2-propanol.

Scheme 3-2. Synthesis of dihydrazones **2** and **3**.

Tetrahydrazones **6** and **7** were synthesized in a similar manner through a three-step procedure. *N*-phenyl-4-[(2-phenylhydrazinylidene)methyl]-*N*-{4-[(2-phenyl-hydrazinylidene)methyl]phenyl}aniline (**4**) was obtained by condensation of 4,4'-diformyltriphenylamine with phenylhydrazine in mixture of THF and 2-propanol (1:1 v/v) as seen in the scheme **3-3**.
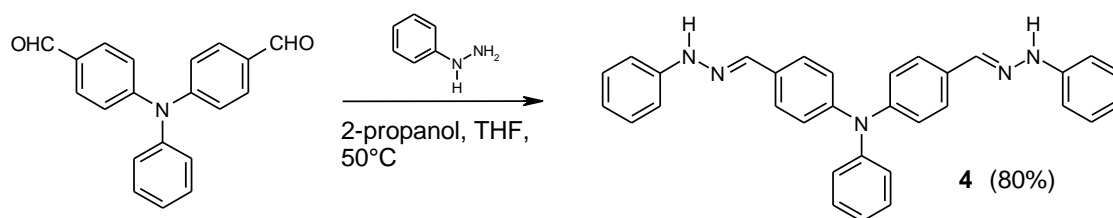
Scheme 3-3. Synthesis of *N*-phenyl-4-[(2-phenylhydrazinylidene)methyl]-*N*-{4-[(2-phenyl-hydrazinylidene)methyl]phenyl}aniline (**4**).

There was a number of attempts to synthesize 4,4'-[(phenylimino)bis{benzene-4,1-diyl(methylylidene[(1-phenylhydrazin-1-yl-2-ylidene]}]dibenzaldehyde (**5**). Finally the goal was achieved by reaction of *p*-fluorobenzaldehyde with hydrazone **4** in anhydrous DMF, under argon, in the presence of base K_2CO_3 (scheme **3-4**).
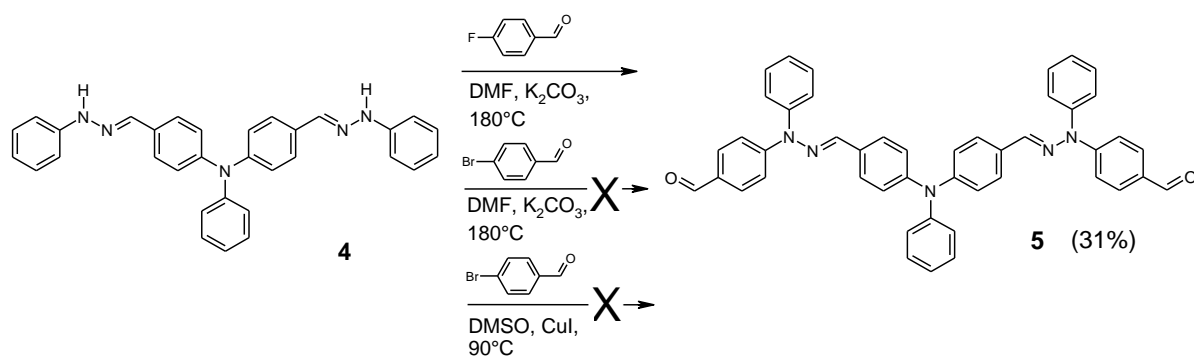
Scheme 3-4. Synthesis of 4,4'-[(phenylimino)bis{benzene-4,1-diyl(methylylidene[(1-phenylhydrazin-1-yl-2-ylidene]}]dibenzaldehyde (**5**).

Dialdehyde **5** was used in two condensation reactions: with 1-methyl-1-phenylhydrazine and 1,1-diphenylhydrazine yielding 4-[(2-{4-[(2-methyl-2-phenylhydrazinylidene)methyl]phenyl}-2-phenylhydrazinylidene)methyl]-*N*-{4-[(2-{4-[(2-methyl-2-phenylhydrazinylidene)methyl]phenyl}-2-phenylhydrazinylidene)methyl]phenyl}-*N*-phenylaniline (**6**) and 4-[(2-{4-[(diphenylhydrazinylidene)methyl]phenyl}-2-phenylhydrazinylidene)methyl]-*N*-{4-[(2-{4-[-(diphenylhydrazinylidene)methyl]phenyl}-2-phenylhydrazinylidene)methyl]phenyl}-*N*-phenylaniline (**7**) accordingly. The reactions were carried out in a (2:1 v/v) solution of toluene and 2-propanol with a catalytic amount of acetic acid as demonstrated in scheme **3-5**.
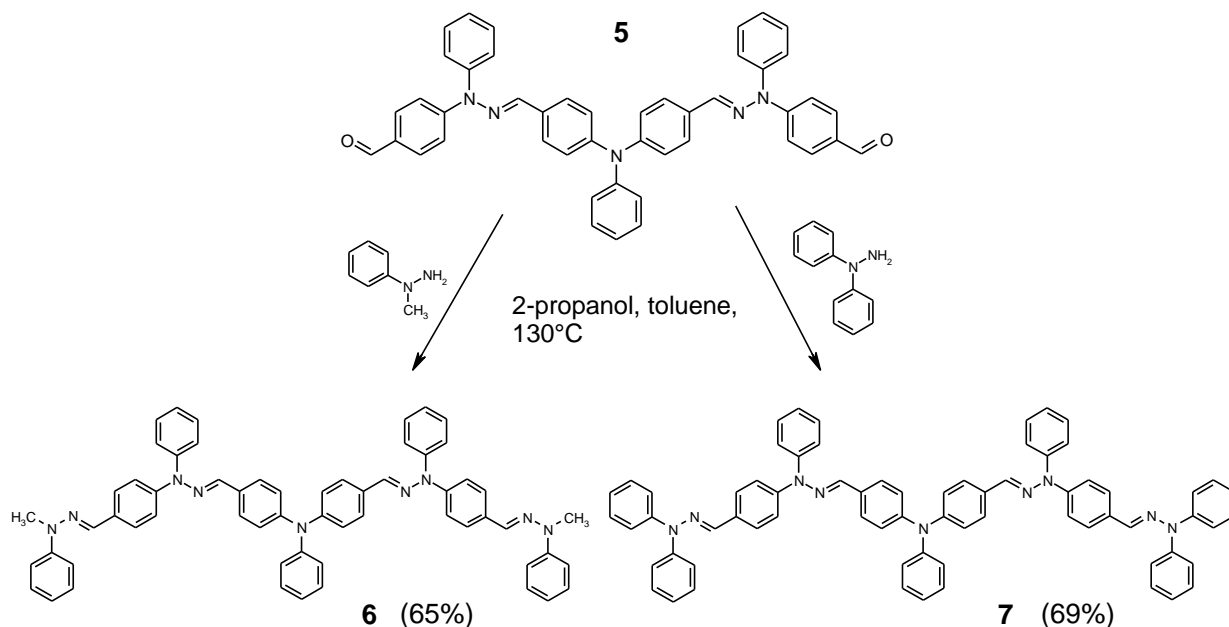
Scheme 3-5. Synthesis of tetrahydrazones **6** and **7**.

Methoxy analogues were synthesized in a similar manner as hydrazones **2**, **3** and **6**, **7**. The first step was condensation of 4-[*N,N*-bis(4-bromophenyl)amino]benzaldehyde with phenylhydrazine in THF to afford 4-bromo-*N*-(4-bromophenyl)-*N*-{4-[(2-phenylhydrazinylidene)methyl]phenyl}aniline (**8**) (Scheme **3-6**).
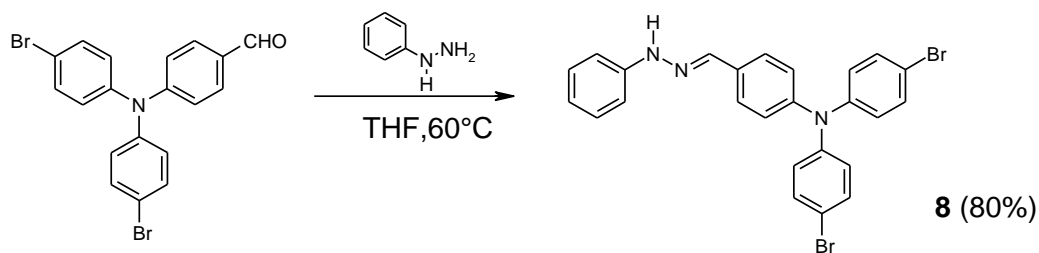
Scheme 3-6. Synthesis of 4-bromo-*N*-(4-bromophenyl)-*N*-{4-[(2-phenylhydrazinylidene)methyl]phenyl}aniline (**8**).

Hydrazone **8** was used in a reaction with *p*-fluorobenzaldehyde in anhydrous DMF under argon and in the presence of K₂CO₃ to yield 4-[2-{4-[bis(4-bromophenyl)amino]benzylidene}-1-phenylhydrazinyl]benzaldehyde (**9**). Consequently aldehyde **9** was condensed with 1-methyl-1-phenylhydrazine and 1,1-diphenylhydrazine in toluene and 4-bromo-*N*-(4-bromophenyl)-*N*-{4-[(2-{4-[(2-methyl-2-phenylhydrazinylidene)methyl]phenyl}-2-phenylhydrazinylidene)methyl]phenyl}aniline (**10**) and 4-bromo-*N*-(4-bromophenyl)-*N*-{4-[(2-{4-[(diphenylhydrazinylidene)methyl]phenyl}-2-phenylhydrazinylidene)methyl]phenyl}aniline (**11**) were isolated accordingly (Scheme **3-7**).
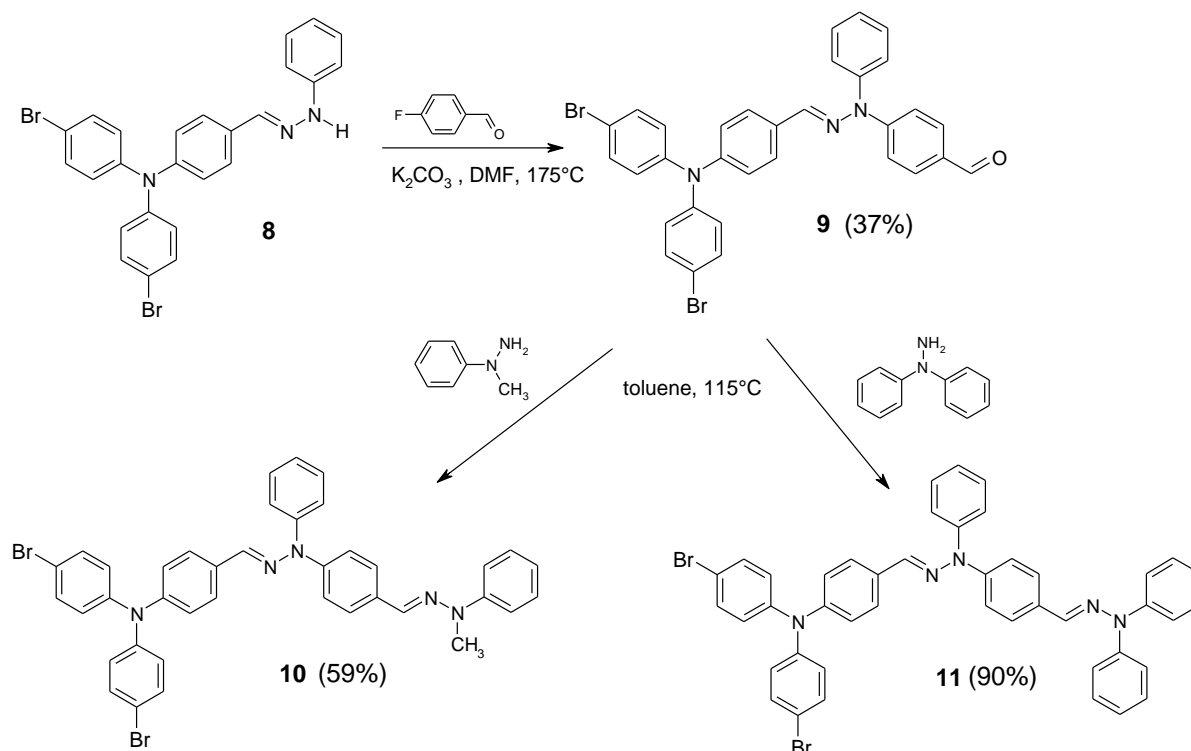
Scheme 3-7. Synthesis of aldehyde **9**, hydrazone **10**, **11**.

The final step of the synthesis was substitution of the bromines with methoxy moieties. It was done by reacting the according hydrazone with a sodium methoxide solution in methanol to yield 4-methoxy-*N*-(4-methoxyphenyl)-*N*-{4-[(2-{4-[(2-methyl-2-phenylhydrazinylidene)methyl]phenyl}-2-phenylhydrazinylidene)methyl]phenyl}aniline (**12**) and 4-[2-{4-[(diphenylhydrazinylidene)methyl]phenyl}-2-phenylhydrazinylidene)methyl]-*N,N*-

17

bis(4-methoxyphenyl)aniline (**13**). The reaction was carried out under argon in anhydrous DMF in a presence of the catalyst CuI (scheme **3-8**).

12 R: −CH₃ **13 R:** ⟨phenyl⟩

Scheme 3-8. Synthesis of hydrazones **12** and **13**.

Tetrahydrazones with a methoxy moiety were synthesized in a four step synthesis procedure, the first of which was the condensation of phenylhydrazine with 4,4'-diformyl-4"-bromotriphenylamine in a THF and 2-propanol (2:1 v/v) to obtain 4-bromo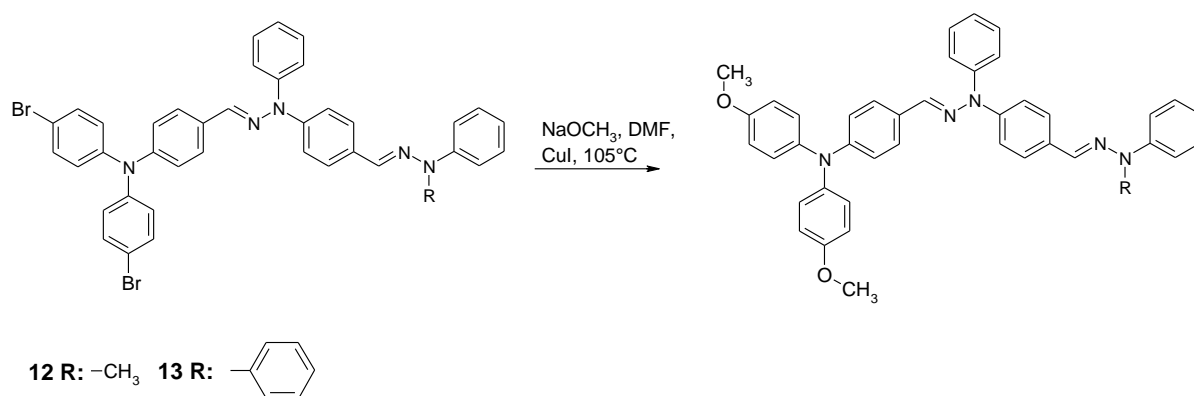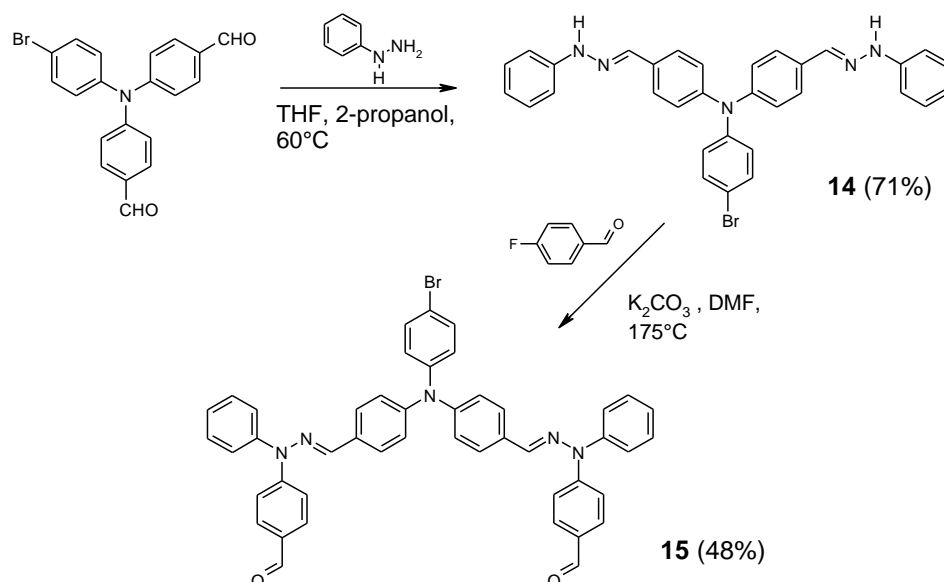-*N,N*-bis{4-[(2-phenylhydrazinylidene)methyl]phenyl}aniline (**14**). The resulting hydrazone **14** was used in a reaction with *p*-fluorobenzaldehyde in anhydrous DMF under argon in the presence of K₂CO₃ base to obtain 4,4'-([(4-bromophenyl)imino]bis{benzene-4,1-diylmethylylidene[1-phenylhydrazin-1-yl-2-ylidene]})dibenzaldehyde (**15**) (scheme **3-9**).

Scheme 3-9. Synthesis of hydrazone **14** and aldehyde **15**.

Aldehyde **15** was used in the reactions with 1-phenyl-1-methylhydrazine and 1,1-diphenylhydrazine in toluene resulting in formation of 4-bromo-*N*-{4-[(2-{4-[(2-methyl-2-phenylhydrazinylidene)methyl]phenyl}-2-phenylhydrazinylidene)methyl]phenyl}-*N*-{4-[(2-{4-[(2-methyl-2-phenylhydrazinylidene)methyl]phenyl}-2-phenylhydrazinylidene)methyl]phenyl}aniline (**16**) and 4-bromo-*N,N*-bis{4-[(2-{4-

18

[(diphenylhydrazinylidene)methyl]phenyl}-2-phenylhydrazinylidene)methyl]phenyl}aniline (**17**) accordingly (scheme **3-10**).
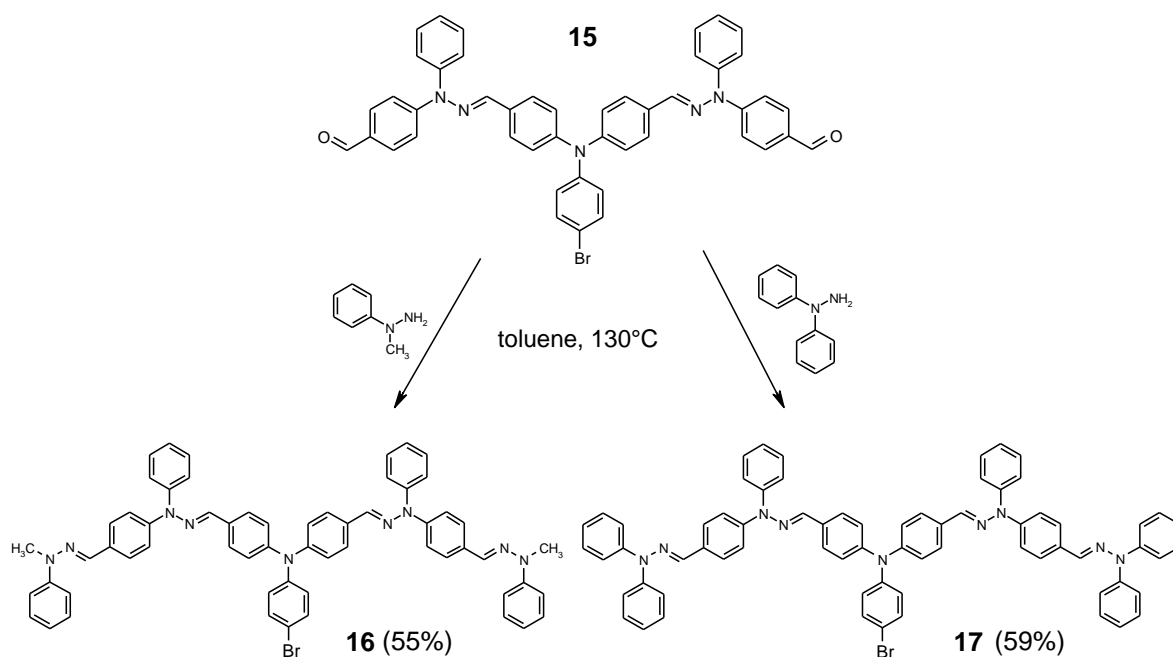
Scheme 3-10. Synthesis of hydrazones **16** and **17**.

As with the methoxy containing dihydrazones **12** and **13**, the last step of the synthesis procedure of the tetrahydrazone **18** was substitution of bromine with a methoxy moiety. 4-methoxy-*N*-{4-[(2-{4-[(2-methyl-2-phenylhydrazinylidene)methyl]phenyl}-2-phenylhydrazinylidene)methyl]phenyl}-*N*-{4-[(2-{4-[(2-methyl-2-phenylhydrazinylidene)methyl]phenyl}-2-phenylhydrazinylidene)methyl]phenyl}aniline   (**18**) was synthesized in the same manner as hydrazone **12**. 4-[(2-{4-[(diphenylhydrazinylidene)methyl]phenyl}-2-phenylhydrazinylidene)methyl]-*N*-{4-[(2-{4-[(diphenylhydrazinylidene)methyl]phenyl}-2-phenylhydrazinylidene)methyl]phenyl}-*N*-(4-methoxyphenyl)aniline (**19**) however, could not be obtained in the same way and a number of different synthesis methods have been investigated. It was attempted to conduct the reaction under pressure in a closed pressure vessel and also under microwave irradiation without pressure, both methods yielded no results. Ultimately, the only successful synthetic path was to conduct the reaction under microwave irradiation and pressure (4 bar), but even then the yield was rather low. The poor yield could be explained by the bulkiness of the molecule and the many possible twists around single bonds which allow the molecules to arrange itself spatially in a way that hinders access to the bromine. The microwave irradiation possibly forces the segments of molecules to arrange themselves differently thus easing access to the reaction site. The aforementioned reactions are shown in the scheme **3-11**.
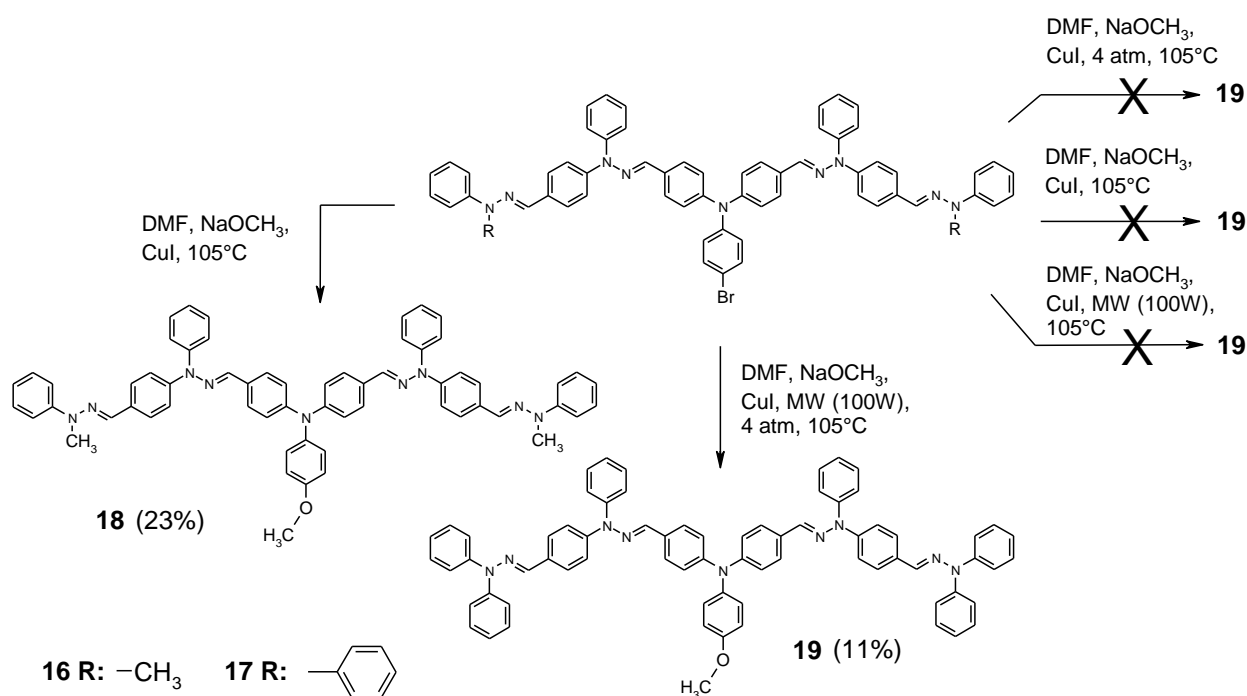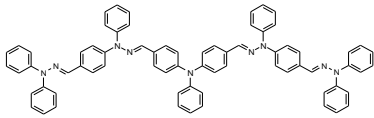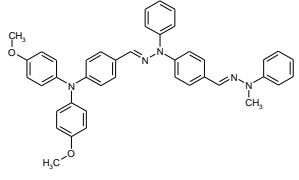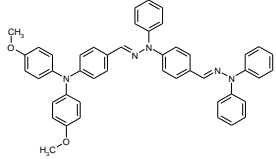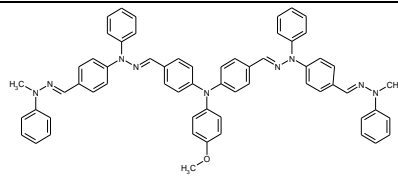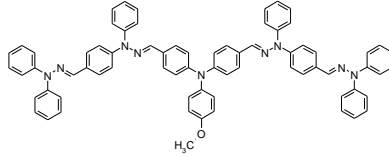
Scheme 3-11. Synthesis of hydrazones **18** and **19**.

3.2 Thermal, optical and photoelectric properties of synthesized materials

The properties of synthesized materials were studied using a number of methods, the most important characteristics are presented in the table below. The various tendencies of these parameters will be discussed further within this section. A description of used methods can be found in the experimental details section.

Table 3-1. thermal properties and UV-vis absorbtiom maxima of the synthesized HTMs.

Structure	T_g, C°	T_m, C°	λ_A, nm
  2	42	182	392
  3	89	129	395
  6	95	-	406

Structure	T_g, C°	T_m, C°	λ_A, nm
7	100	-	397
12	45	142	396
13	69	182	400
18	105	-	415
19	85	-	409

In order to evaluate the size of the conjugated π-electron systems within the synthesized molecules UV-vis absorption spectra were recorded. Knowledge of the relative size of the conjugated system allows approximate predictions of certain parameters, like the hole drift mobility.

There are several tendencies worth mentioning when exploring the presented UV-vis spectra. First of all the introduction of methoxy moieties causes a batochromic shift for most structures (4 nm for **2** and **12**, 5 nm for **3** and **13**, 9 nm for **6** and **18**, 12 nm for **7** and **19**). It can be explained by the increased electron density in the conjugated system due to the electron donating properties of the methoxy moiety. The other tendency is batochromic shifts caused by adding more aromatic fragments. For example dihydrazones **3** and **13** have an UV- vis absorption maximum at 395 nm and 400 nm *versus* 392 nm and 396 nm for dihydrazones **2** and **12** due to the additional phenyl ring in the hydrazone fragment.
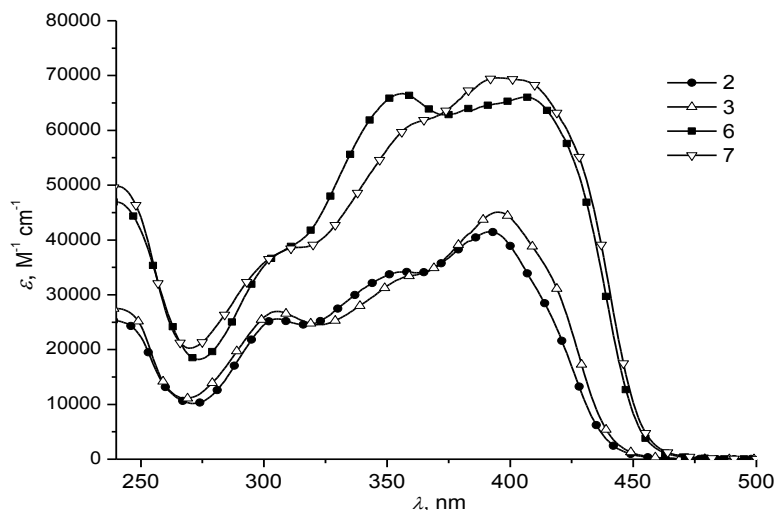
Figure 3-1. UV-vis absorbption maxima of HTMs **2**, **3**, **6**, **7**.
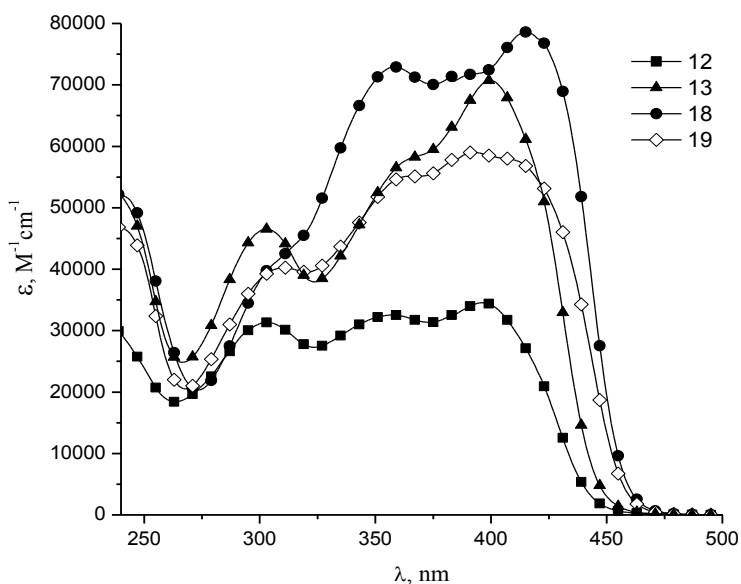
Figure 3-2. UV-vis absorbption maxima of HTMs **12**, **13**, **18**, **19**.

A hyperchromic shift can also be observed in the tetrahydrazones **6**, **7**, **18** relative to the dihydrazones (**2**, **3**, **12**, **13**). It can be explained by a significant increase in size of the molecules which in turn increases the statistical probability of absorbing photons and also by a change in electron distribution caused by the methoxy moieties.

Tetrahydrazones **13** and **19** display electromagnetic wave absorption maximums at lower wavelengths than could be expected. This could be attributed to their bulky structures and several double bonds which allow for many steric isomers and rotations around phenyl rings which allow for many less planar conformations.

The ability to form stable and flexible amorphous layers is an important quality for the HTMs used in solid state organic and hybrid solar cells. The ability to do so can be quantified by

the material's glass transition temperature. In order to explore the morphological properties and stability, differential scanning calorimetry has been used. The general tendency observed is in accordance with Wirth's postulates – adding large, rigid moieties increases T_g thus increasing the stability of the amorphous glassy state. This is well demonstrated by a significant increase of T_g (47°C for dihydrazones **2**, **3** and 24°C for dihydrazones **12**, **13**) when a single methyl moiety is substituted by a phenyl ring. Tetrahydrazones have an even higher T_g and are completely amorphous, however presence of a large number of different conformations lessen the effect of the additional phenyl rings within the hydrazone moieties and the influence of exchange of methyl for a phenyl fragment.

One of the key qualities of an HTM is hole drift mobility. It was studied by the xerographic time-of-flight (XTOF) method. The most important HTM photophysical parameters, such as hole mobility (μ), zero field mobility (μ_0), Poole–Frenkel parameter (α) are presented in the table **3-2**. The hole drift mobility of dihydrazones **2**, **3** is a whole order of magnitude higher than that of methoxy substituted dihydrazones **12**, **13** and tetrahydrazones **6**, **7**. Worse performance of **6**, **7**, **12**, **13** can be attributed to the less orderly packing of molecules within amorphous layers caused by the presence of methoxy or additional hydrazone moieties. Structural disorder in films hinders charge hoping between molecules. Methoxy substituted tetrahydrazones **18**, **19** demonstrate the best hole drift mobility (up to 2.5×10^{-3} cm^{2}V^{-1}s^{-1}), drift mobility of this order of magnitude could be considered rather high in comparison with that of the many published organic molecular HTMs [40]. This might be explained by the improved molecule packing within the films fabricated using these materials.
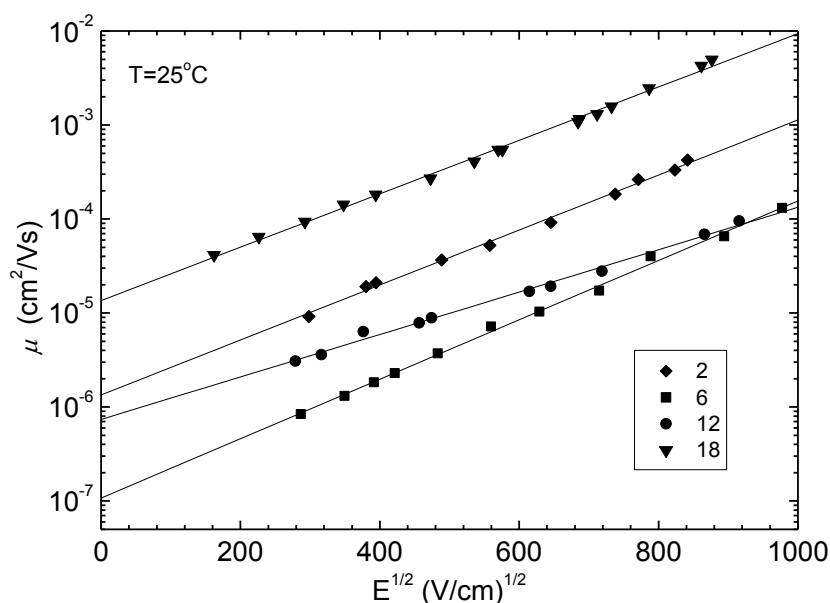

Figure 3-3. Hole drift mobilities of HTMs **2**, **6**, **12**, **18**.

Table 3-2. Optoelectric properties of the HTMs.

Structure	$^*\mu^a$, cm^{2}V^{-1}s^{-1}	μ_0, cm^{2}V^{-1}s^{-1}	α	d, μm	E_{ox}, V vs NHE [b]	I_p, eV*
2	2.9×10^{-4}	1.4×10^{-6}	0.0067	3.4	0.97	5.26
3	5.6×10^{-4}	1.1×10^{-6}	0.0078	3.4	0.80	5.22
6	3.6×10^{-5}	1×10^{-7}	0.0073	4.5	0.93	5.17
7	3.6×10^{-5}	1.4×10^{-7}	0.007	4.3	0.88	5.17
12	4.7×10^{-5}	7×10^{-7}	0.0052	3.6	0.74	5.16
13	4.6×10^{-5}	7×10^{-7}	0.0054	3.4	0.77	5.22
18	2.5×10^{-3}	1.4×10^{-5}	0.0065	7.6	0.77	5.15
19	2.4×10^{-3}	6.5×10^{-5}	0.007	2.7	0.76	5.10

[a] The presented hole mobility values (μ) are the values observed at an electric field of 6.4×10^5 Vcm^{-1}. [b] CV measurements were carried out at a glassy carbon electrode in dichloromethane solutions containing 0.1 M tetrabutylammonium hexafluorophosphate as electrolyte and Ag/AgNO$_3$ as the reference electrode. Each measurement was calibrated with ferrocene (Fc). Potentials measured vs Fc$^+$/Fc were converted to normal hydrogen electrode (NHE) by addition of +0.7 V. *Measurements were carried out at the department of solid state electronics, Vilnius University.

Electrochemical characteristics of the HTMs have been explored using cyclic voltammety (CV). Judging from the voltammograms all the synthesized materials demonstrate quasireversible oxidation-reduction couples, indicating that the materials undergo reversible oxidation-reduction cycles (figure **3-4**). Oxidation potentials determined by CV do not indicate any absolute solid-state ionization energy values, but can be used to compare various compounds relative to one another. A more important parameter when considering the construction of photovoltaic devices is the solid-state ionization potential of the substance (I_p), determined using electron photoemission in air method (figure **3-5**).
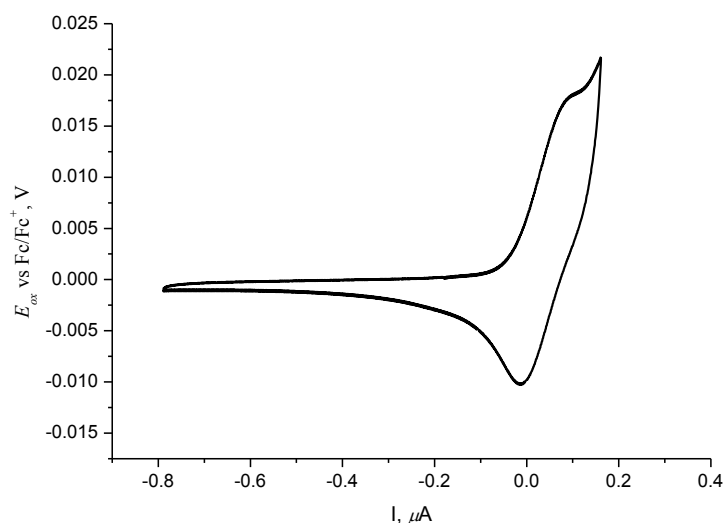
Figure 3-4. HTM **18** voltammogram.

Overall, modification of the hydrazones in order to reduce their I_p and make them more viable as HTMs for ssDDSC and perovskite based solar cell devices was successful − the introduction of methoxy moieties allowed to reach E_{ox} values as low as 0.74 V vs NHE and I_p as low as 5.1 eV which is not that far from the corresponding parameters of the most effective HTM spiro-MeOTAD ($E_{ox} = 0.69$ V vs NHE; $I_p = 5.0$ eV). However it is hard to verify the extent to which each introduced moiety affected these parameters of the explored HTMs. There are also minor deviations in the tendencies of E_{ox} and I_p changes. This, most likely, is caused by the additional interactions between molecules within a solid layer.
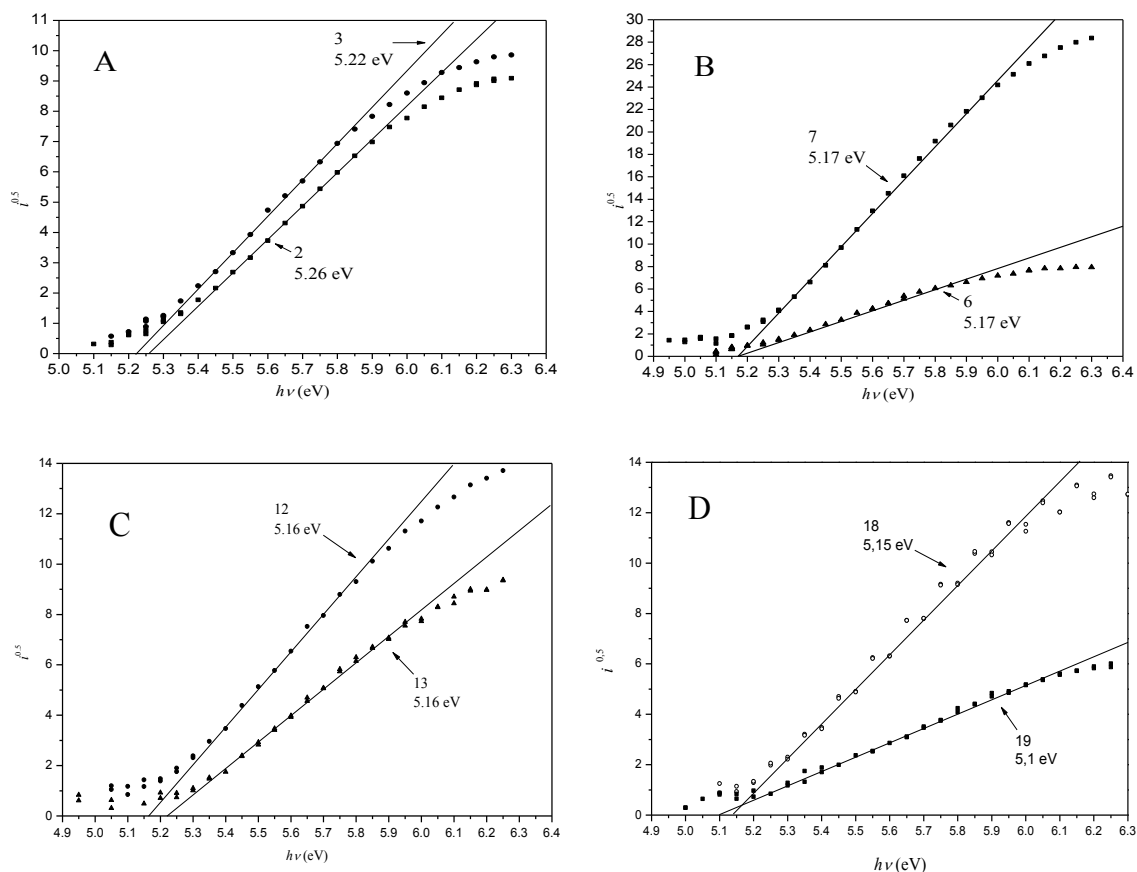
Figure 3-5. I_p of the HTMs (A) **2**, **3**; (B) **6**, **7**; (C) **12**, **13**; (D) **18**, **19**.

The ultimate goal of this work was to test the synthesized HTMs in the ssDSSC and perovskite based solar cells. HTMs **2**, **3**, **6**, **7**, **12**, **13**, **18** were used to fabricate solid state dye-sensitized solar cells and HTMs **12**, **18** were also used to fabricate perovskite based solar cells. The results of characterization of the devices are shown in the table **3-3**. The presented values are as follows: short circuit current (J_{sc}), open circuit voltage (V_{oc}), fill factor (*FF*) and solar energy to electricity conversion efficiency (η).

Table 3-3. Parameters of the devices fabricated using investigated HTMs*.

Structure	Device type	J_{sc}, mA cm^{-2}	V_{oc}, V	FF, %	η, %
2	ssDSSC	2.38	0.54	34	0.4
3	ssDSSC	2.52	0.66	40	0.7
6	ssDSSC	1.64	0.64	30	0.3
7	ssDSSC	1.78	0.6	33	0.3
12	ssDSSC	0.69	0.52	46	0.2
13	ssDSSC	3.35	0.82	36	1
18	ssDSSC	5.59	0.68	42	1.6
12	PSC	6.19	0.46	35	1
18	PSC	4.83	0.84	26	1.1

* Device fabrication and characterization has been carried out at BASF SE.

The methoxy substituted tetrahydrazone **18** showed the best performance in ssDSSC devices at 1.6% efficiency and the better performance of the two HTM tested in perovskite based solar cells (1.1%). Judging from the preliminary testing results the doping procedures used for spiro-MeOTAD are not that suitable for these materials. Most likely higher ionization potential of the investigated hydrazones hampers the doping process and the conductivity remains low, which is evident from rather low fill factor. Further optimization of the doping procedure and device construction is necessary in order to enhance the performance of these HTMs in solar cells.

4. Experimental details

4.1 General Methods and Materials

Chemicals were purchased from Sigma-Aldrich and TCI Europe and used as received without further purification. 4-[*N*,*N*-Bis(4-bromophenyl)amino]benzaldehyde was synthesized according to an earlier reported procedure [41]. The ^{1}H and ^{13}C NMR spectra were taken on Varian Unity Inova (300 MHz), Bruker Avance III 400 (400 MHz) and Bruker Avance III 700 (700 MHz) spectrometers at room temperature. The chemical shifts, expressed in δ (ppm) are relative to a $(CH_3)_4Si$ (TMS, 0 ppm) internal standard. The course of the reactions products were monitored by TLC on ALUGRAM SIL G/UV254 plates and developed with I_2 or UV light. Silica gel (grade 9385, 230–400 mesh, 60 Å, Aldrich) was used for column chromatography. Elemental analysis was performed with an Exeter Analytical CE-440 elemental analyzer, Model 440 C/H/N/. Differential scanning calorimetry (DSC) was performed on a Q10 calorimeter (TA Instruments) at a scan rate of 10 K/min in the nitrogen atmosphere. The glass transition temperatures for the investigated compounds were determined during the second heating scan. UV/Vis spectra were recorded on a PerkinElmer Lambda 35 spectrometer.

Cyclic Voltammetry Measurements (CV)

Electrochemical studies were carried out by a three-electrode assembly cell and potentiostat-galvanostat from Bio-Logic SAS. Measurements were carried out with a glassy carbon electrode in dichloromethane solutions containing 0.1 M tetrabutylammonium hexafluorophosphate as electrolyte, $Ag/AgNO_3$ as the reference electrode, and a Pt wire counter electrode.

Ionization-potential measurements (I_p)

The ionization potential (I_p) of the layers of the synthesized compounds was measured by electron photoemission in air. The samples were prepared by dissolution in $CHCl_3$ and the solutions were coated on Al plates pre-coated with approximately 0.5 μm thickness of a methylmethacrylate and methacrylic acid copolymer adhesive layer. The thickness of the transporting material layer was 0.5 – 1 μm. The organic materials investigated are stable enough to oxygen that the measurements may be carried out in the presence of air. The samples were illuminated with monochromatic light from a quartz monochromator fitted with a deuterium lamp. The power of the incident light beam was $(2–5) \cdot 10^{-8}$ W. A negative voltage (-330 V) was supplied to the sample substrate. The counter electrode with a $4.5 \cdot 15$ mm^2 slit for illumination was placed 8 mm from the sample surface. The counter electrode was connected to the input of the BK2–16 type electrometer, working in the open input regime, for the photocurrent measurement. The $10^{-15} – 10^{-12}$ A photocurrent (*I*) flowed in the circuit under illumination. The

value of I is strongly dependent on the incident-light photon energy (hv). The dependence $I^{0.5}$ on incident-light quanta energy hv was plotted from the experiment results. Usually the dependence of I on the incident light quantum energy is described well by the linear relationship $I^{0.5} = f(hv)$ near the threshold. The linear part of this dependence was extrapolated to the hv axis and the I_p value was determined as the photon energy at the interception point.

Hole-drift-mobility measurements

The samples for the hole-drift-mobility measurements were prepared by spin coating solutions of the synthesized compounds in toluene onto PS films with a conductive Al layer. The layer thickness was in the range $5 - 10$ μm. The hole drift mobility was measured by XTOF. An electric field was created by positive corona charging. The charge carriers were generated at the layer surface by illumination with pulses of a nitrogen laser (pulse duration = 2 ns, $\lambda = 337$ nm). The layer surface potential decrease as a result of pulse illumination was up to 1–5% of the initial potential before illumination. The capacitance probe that was connected to the wide-frequency band electrometer measured the speed of the surface potential decrease (dU/dt). The transit time (t_t) was determined by the kink on the curve of the dU/dt transient on a linear or double logarithmic scale. The drift mobility was calculated by the formula $\mu = d^2/U_0 t_t$ (d is the layer thickness, U_0 is the surface potential at the moment of illumination).

ssDSSC fabrication and characterization

A TiO_2 blocking layer was prepared on a fluorine-doped tin oxide (FTO)-covered glass substrate using spray pyrolysis. Next, a TiO_2 paste (Dyesol), diluted with terpineol, was applied by screen printing, resulting in a film 1.7 µm thick. All films were then sintered for 45 min at 450 °C, followed by treatment in a 40 mM aqueous solution of $TiCl_4$ at 60 °C for 30 min, followed by another sintering step. The prepared samples with TiO_2 layers were pretreated with 5 mM solutions of 2-(p-butoxyphenyl)acetohydroxamic acid sodium salt in ethanol. The electrodes were then dyed in 0.5 mM dye N-(9,9-dimethylfluoren-2-yl)-9,9-dimethyl-N-(4-perylenmonoimide-3-ylphenyl)fluoren-2-amine (ID504) solution in CH_2Cl_2. 200 nm thick layer of hole transporting material was applied by spin-coating from a solution in chlorobenzene (200mg/ml) also containing 33 µl/ml of $Li(CF_3SO_2)_2N$ (LiTFSI) solution in cyclohexanone (stock solution concentration 127 mg/ml). Fabrication of the device was completed by evaporation of 200 nm of silver as the counter electrode. The active area of the solid state DSSC was defined by the size of these contacts (0.13 cm^2), and the cells were masked by an aperture of the same area for measurements. The Current–voltage characteristics for all cells were measured with a Keithley 2400 under 1000 W m^{-2}, AM 1.5G conditions (LOT ORIEL 450 W).

Perovskite solar cell fabrication and characterization

The solar cells were built on NSG10 glass and a 30-50nm thick TiO_2 blocking layer wass produced by spray pyrolysis. The mesoporous TiO_2 (150mg 30NRD Dyesol paste per 1 ml of EtOH) layer was applied by spin-coating for 20 s (5000rpm, 2000rpm/s) and annealed at 500°C for 15 min. 1.1M PbI_2 /MAI (1:1) in DMSO was spin coated using chlorobenzene as an antisolvent. The perovskite layer was deposited inside a Nitrogen glovebox. The hole transporting material was applied by spin-coating for 20 s at 4000 rpm from a chlorobenzene solution (16.1mg in 400µl, 30mmol) using LiTFSI (3.5µl from a 520mg/ml stock solution in acetonitrile). Fabrication of the device was completed by evaporation of 90 nm of gold as the counter electrode. The Current–voltage characteristics for all cells were measured with a Keithley 2400 under 1000 W m^{-2}, AM 1.5G conditions (LOT ORIEL 450 W).

4.2 Description of synthesis
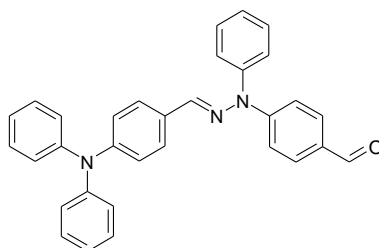
4-{2-[4-(diphenylamino)benzylidene]-1-phenylhydrazinyl}benzaldehyde (1): 10 g (27.5 mmol) of 4-(diphenylamino)benzaldehyde diphenylhydrazone, 11.4 g (82.5 mmol) K_2CO_3 and 4.43 mL (41.25 mmol) *p*-fluorobenzaldehyde were dissolved in 100 mL of anhydrous DMF, under argon atmosphere. The mixture was heated for 48 hours at reflux. After termination of the reaction (TLC toluene/ethyl acetate/*n*-hexane = 8:2:15) the mixture was extracted with ethyl acetate. The organic layer was dried over anhydrous Na_2SO_4, filtered, the solvent was removed. The crude product was purified by column chromatography (1:10:14 v/v ethyl acetate/toluene/*n*-hexane) to give **1** as an orange amorphous mass (4.473 g, 35%). ^{1}H NMR (300MHz, CDCl$_3$, 25°C, TMS): 9.80 (s, 1H), 7.72 (d, *J* = 9.0 Hz, 2H), 7.67 − 7.44 (m, 5H), 7.29 − 7.13 (m, 10H), 7.13 − 6.99 (m, 7H) ppm; ^{13}C NMR (CDCl$_3$, 75MHz, 25°C, TMS): 190.85, 148.82, 147.33, 138.96, 131.50, 131.23, 129.98, 129.54, 129.46, 129.14, 128.91, 128.77, 128.33, 127.82, 124.93, 123.54, 122.85, 114.15 ppm;

Elemental analysis calcd (%) for $C_{32}H_{25}N_3O$: C 82.20, H 5.39, N 8.99; found: C 82.32, H 5.61, N 8.71.
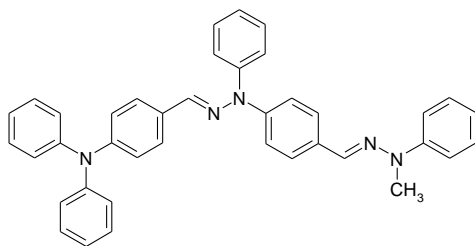
4-[(2-{4-[(2-methyl-2-phenylhydrazinylidene)methyl]phenyl}-2-phenylhydrazinylidene)methyl]-*N,N*-diphenylaniline (2): 0.537 g (1.148 mmol) of aldehyde **1** was dissolved in mixture of toluene and isopropanol (4.5mL, 2:1, v/v), 0.167 mL (1.378 mmol) 1-phenyl-1-methylhydrazine and a catalytic amount of acetic acid were added. The mixture was heated for 1.5 hours at reflux after which the reaction was terminated and the solvent removed (TLC diethyl ether/*n*-hexane = 6:19). The crude product was purified by column chromatography (0.6:24.4 v/v diethylether/*n*-hexane) to give **2** as a bright yellow solid (0.51 g, 78%). ^{1}H NMR (300MHz, CDCl$_3$, 25°C, TMS): 7.70 (d, *J* = 8.7 Hz, 2H), 7.52 − 7.13 (m, 19H), 7.13 − 6.95 (m, 8H), 6.91 (t, *J* = 7.0 Hz, 1H), 3.40 (s, 3H) ppm; ^{13}C NMR (CDCl$_3$, 75MHz, 25°C, TMS): 148.00, 147.56, 144.04, 142.93, 135.91, 132.28, 131.73, 130.24, 130.11, 129.40, 129.14, 127.41, 127.33, 125.38, 124.64, 124.08, 123.46, 123.20, 121.14, 120.48, 115.21, 115.14, 33.18 ppm;

Elemental analysis calcd (%) for C$_{39}$H$_{33}$N$_5$: C 81.93, H 5.82, N 12.25; found: C 81.85, H 6.02, N 12.13.
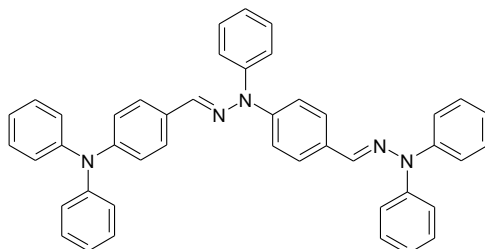
4-[(2-{4-[(diphenylhydrazinylidene)methyl]phenyl}-2-phenylhydrazinylidene)methyl]-*N,N*-diphenylaniline (3): 0.93 g (1.99 mmol) of aldehyde **1** was dissolved in mixture of toluene and isopropanol (6 mL, 1:1, v/v). 0.739 g (3.25 mmol) of 1,1-diphenylhydrazine hydrochloride were extracted with toluene and a saturated water solution of K$_2$CO$_3$. The organic layer was added into the reaction mixture together with a catalytic amount of acetic acid. The mixture was heated for 3 h at reflux after which the reaction was terminated and the solvent removed (TLC diethyl ether/*n*-hexane = 6:19). The crude product was purified by column chromatography (0.75:24.25 v/v diethylether/*n*-hexane) to give **3** a bright yellow solid (0.747 g, 59%). ^{1}H NMR (300MHz, CDCl$_3$, 25°C, TMS): 7.60 (s, 1H), 7.57 (s, 1H), 7.49 − 7.36 (m, 8H), 7.29 − 6.97 (m, 25H) ppm; ^{13}C NMR (CDCl$_3$, 75MHz, 25°C, TMS): 148.08, 147.57, 144.82, 143.89, 142.51, 136.08, 135.53, 131.20, 130.21, 129.89, 129.41, 127.62, 127.36, 125.84, 124.83, 124.68, 124.49, 123.44. 123.23, 122.62, 120.35 ppm;

Elemental analysis calcd (%) for $C_{44}H_{35}N_5$: C 83.38, H 5.57, N 11.05; found: C 83.50, H 5.33, N 11.17.
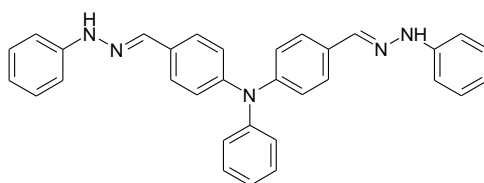
_N_-phenyl-4-[(2-phenylhydrazinylidene)methyl]-_N_-{4-[(2-phenyl-hydrazinylidene)methyl]phenyl}aniline (4): 4.5 g (14.93 mmol) of 4,4'-diformyltriphenylamine was dissolved in a mixture of tetrahydrofurane and isopropanol (45 mL, 1:1, v/v). 3.68 mL (39.185 mmol) of phenylhydrazine were slowly added into the mixture while stirring (TLC acetone/_n_-hexane = 5:20). Crystals, formed during the reaction, were filtered and washed with a (1:1, v/v) mixture of _n_-hexane and isopropanol to give **4** as yellow crystals (5.77 g, 80%). Hydrazone **4** was used in the next step without purification.
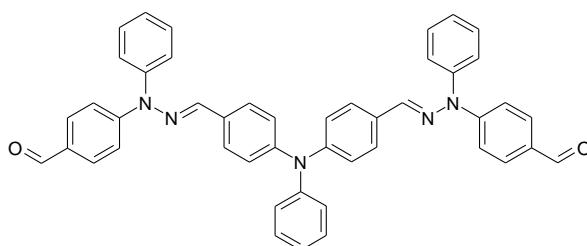
Synthesis of 4,4'-[(phenylimino)bis{benzene-4,1-diyl(methylylidene[(1-phenylhydrazin-1-yl-2-ylidene]}]dibenzaldehyde (5): 2.61 g (5.42 mmol) of hydrazone **4**, 4.494 g (32.14 mmol) K_2CO_3 and 1.74 mL (16.22 mmol) _p_-fluorobenzaldehyde were dissolved in 100 mL of anhydrous DMF, under argon atmosphere. The mixture was heated for 24 h at reflux. After termination of the reaction (TLC acetone/_n_-hexane = 5:20), the mixture was extracted with ethyl acetate. The organic layer was dried over anhydrous Na_2SO_4, filtered, the solvent was removed. The crude product was purified by column chromatography (3:22 v/v acetone/_n_-hexane) to give **5** as a yellow solid (1.159 g, 31%). ^{1}H NMR (300MHz, CDCl3, 25°C, TMS): 9.81 (s, 2H), 7.76 − 7.46 (m, 13H), 7.32 − 7.01 (m, 20H) ppm; ^{13}C NMR (CDCl3, 75MHz, 25°C, TMS): 190.86, 152.11, 148.17, 146.88, 138.70, 138.43, 131.50, 131.26, 129.94, 129.76, 129.60, 128.89, 127.90, 127.62, 125.38, 124.16, 123.72, 114.23 ppm;

Elemental analysis calcd (%) for $C_{46}H_{35}N_5O_2$: C 80.09, H 5.11, N 10.15; found: C 80.27, H 5.28, N 9.96.
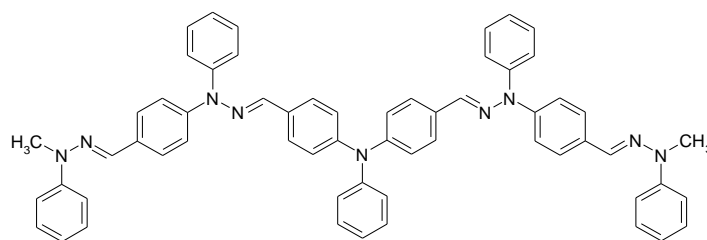
Synthesis of 4-[(2-{4-[(2-methyl-2-phenylhydrazinylidene)methyl]phenyl}-2-phenylhydrazinylidene)methyl]-*N*-{4-[(2-{4-[(2-methyl-2-phenylhydrazinylidene)methyl]phenyl}-2-phenylhydrazinylidene)methyl]phenyl}-*N*-phenylaniline (6): 0.313 g (0.454 mmol) of aldehydesubstance **5** was dissolved in a mixture of toluene and isopropanol (9 mL, 2:1, v/v), 0.15 mL (1.274 mmol) 1-phenyl-1-methylhydrazine and a catalytic amount of acetic acid were added. The mixture was heated for 1 h at reflux after which the reaction was terminated and the solvent removed (TLC ethyl acetate/*n*-hexane = 8:17). The crude product was purified by column chromatography (4:21 v/v ethyl acetate/*n*-hexane) to give **6** as a yellow solid (0.264 g, 65%). ^{1}H NMR (300MHz, CDCl$_3$, 25°C, TMS): 7.70 (d, *J* = 8.7 Hz, 3H), 7.54 – 7.00 (m, 39H), 6.90 (t, *J* = 7.0 Hz, 3H), 3.40 (s, 6H) ppm; ^{13}C NMR (CDCl$_3$, 75MHz, 25°C, TMS): 148.02, 147.58, 147.23, 144.02, 142.93, 135.80, 132.35, 131.72, 130.70, 130.11, 129.47, 129.13, 127.42, 125.41, 124.94, 124.08, 123.92, 123.58, 121.18, 120.49, 115.23, 115.01, 33.18 ppm;

Elemental analysis calcd (%) for C$_{60}$H$_{51}$N$_9$: C 80.24, H 5.72, N 14.04; found: C 79.99, H 5.85, N 14.16.
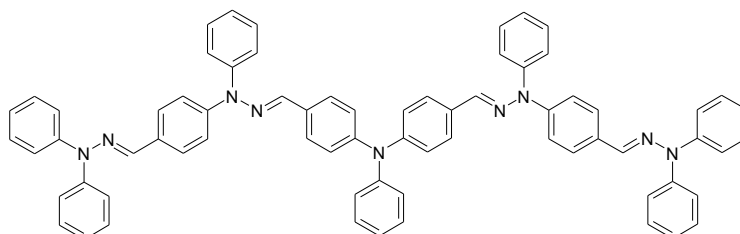
Synthesis of 4-[(2-{4-[(diphenylhydrazinylidene)methyl]phenyl}-2-phenylhydrazinylidene)methyl]-*N*-{4-[(2-{4-[-(diphenylhydrazinylidene)methyl]phenyl}-2-phenylhydrazinylidene)methyl]phenyl}-*N*-phenylaniline (7): 0.256 g (0.371 mmol) of aldehyde **5** was dissolved in a mixture of toluene and isopropanol (6 mL, 1:1, v/v). 0.27 g (1.188 mmol) of 1,1-diphenylhydrazine hydrochloride were extracted with toluene and a saturated water solution of K$_2$CO$_3$. The organic layer was added into the reaction mixture together with a catalytic amount of acetic acid. The mixture was heated for 2 h at reflux after which the reaction was terminated and the solvent removed (TLC ethyl acetate/*n*-hexane = 7:18). The crude product was purified by column chromatography (1.5:23.5 v/v ethyl acetate/*n*-hexane) to give **7** as a yellow solid (0.261 g, 69%). ^{1}H NMR (300MHz, CDCl$_3$, 25°C, TMS): 7.59 (d, *J* = 8.7 Hz, 4H),

7.50 – 7.36 (m, 16H), 7.29 – 7.00 (m, 35H) ppm; ^{13}C NMR (CDCl$_3$, 75MHz, 25°C, TMS): 147.61, 144.76, 143.88, 142.48, 135.93, 135.51, 131.26, 130.63, 130.21, 129.88, 129.48, 129.12, 127.62, 127.40, 125.86, 124.97, 124.80, 124.49, 123.90, 123.61, 122.61, 120.37 ppm;

Elemental analysis calcd (%) for C$_{70}$H$_{55}$N$_9$: C 82.25, H 5.42, N 12.33; found: C 82.01, H 5.55, N 12,44.
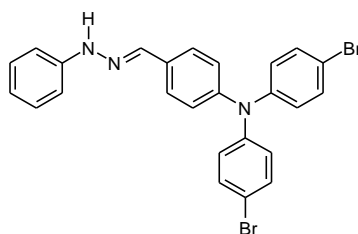
Synthesis of 4-bromo-*N*-(4-bromophenyl)-*N*-{4-[(2-phenylhydrazinylidene)methyl]phenyl}aniline (8): 15 g (34.792 mmol) of 4-[*N*,*N*-Bis(4-bromophenyl)amino]benzaldehyde were dissolved in 100 mL of THF, 4.29 mL (43.49 mmol) of phenylhydrazine were added and the mixture was heated at 60°C for 2 h. After terminating the reaction the solvent was removed and 80 mL of isopropanol was added to the resulting amorphous mass (TLC acetone/*n*-hexane = 3:22). The flask was kept for 30 minutes at -25°C and formed crystals were filtered and washed with a (3:1, v/v) mixture of *n*-hexane and isopropanol to give **8** as yellow crystals (14.51 g, 80%). Hydrazone **8** was used in the next step without purification.
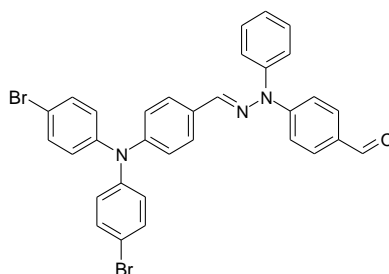
Synthesis of 4-[2-{4-[bis(4-bromophenyl)amino]benzylidene}-1-phenylhydrazinyl]benzaldehyde (9): 14.1 g (27.049 mmol) of hydrazone **8**, 11.22 g (81.149 mmol) K$_2$CO$_3$ and 4.35 mL (40.574 mmol) *p*-fluorobenzaldehyde were dissolved in 100 mL of anhydrous DMF, under argon atmosphere. The mixture was heated for 4.5 h at reflux. After termination of the reaction, the mixture was extracted with ethyl acetate (TLC ethyl acetate/toluene/*n*-hexane = 2:6:17). The organic layer was dried over anhydrous Na$_2$SO$_4$, filtered, the solvent was removed. The crude product was purified by column chromatography (1:7.5:16.5 v/v ethyl acetate/toluene/*n*-hexane) to give **9** as a dark orange amorphous mass (6.23 g, 37%). ^{1}H NMR (700 MHz, CDCl$_3$, 25°C, TMS): 9.82 (s, 1H), 7.74 (d, *J* = 9.0 Hz, 2H), 7.65 (t, *J* = 7.8 Hz, 2H), 7.56 (t, *J* = 7.5 Hz, 1H), 7.51 (d, *J* = 8.7 Hz, 2H), 7.36 (d, *J* = 8.8 Hz, 4H), 7.26 – 7.23 (m, 2H), 7.19 (d, *J* = 8.7 Hz, 2H), 7.16 (s, 1H), 7.01 (d, *J* = 8.6 Hz, 2H), 6.95 (d, *J* =

8.8 Hz, 4H) ppm;^{13}C NMR (176 MHz, CDCl$_3$, 25°C, TMS): 190.89, 152.11, 147.77, 146.16, 138.47, 138.44, 132.66, 131.53, 131.30, 130.27, 129.96, 129.65, 129.05, 128.07, 126.10, 123.66, 116.36, 114.33 ppm;

Elemental analysis calcd (%) for C$_{32}$H23N$_3$Br$_2$O: C 61.46; H 3.71; N 6.72; found: C 61.26; H 3.73; N 6.77.
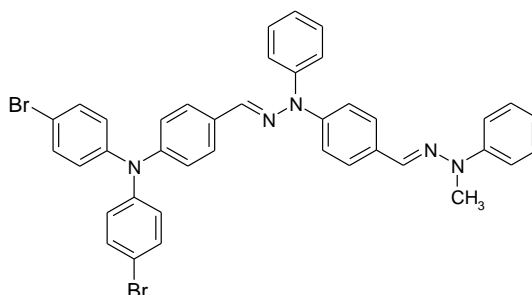
Synthesis of 4-bromo-*N*-(4-bromophenyl)-*N*-{4-[(2-{4-[(2-methyl-2-phenylhydrazinylidene)methyl]phenyl}-2-phenylhydrazinylidene)methyl]phenyl}aniline (10): 1 g (1.599 mmol) of aldehyde **9** was dissolved in 10 mL of toluene, 0.24 mL (2.078 mmol) 1-phenyl-1-methylhydrazine and a catalytic amount of acetic acid were added. The mixture was heated for 1 h at reflux after which the reaction was terminated and the solvent removed (TLC acetone/*n*-hexane = 2:23). The crude product was purified by column chromatography (1:24 v/v acetone/*n*-hexane) to give **10** as a yellow solid (0.691 g, 59%). ^{1}H NMR (400MHz, CDCl$_3$, 25°C, TMS): 7.71 (d, *J* = 8.7 Hz, 2H), 7.60 − 7.09 (m, 19H), 7.08 − 6.87 (m, 7H), 3.43 (s, 3H) ppm;^{13}C NMR (CDCl$_3$, 101MHz, 25°C, TMS): 148.01, 146.88, 146.31, 143.84, 142.88, 135.32, 132.54, 131.64, 131.47, 130.15, 129.16, 127.55, 127.45, 125.82, 125.47, 124.12, 123.97, 121.29, 120.55, 115.94, 115.26, 33.23 ppm;

Elemental analysis calcd (%) for C$_{39}$H$_{31}$N$_5$Br$_2$: C 64.21, H 4.28, N 9.60; found: C 64,26, H 4,21, N 9,57.
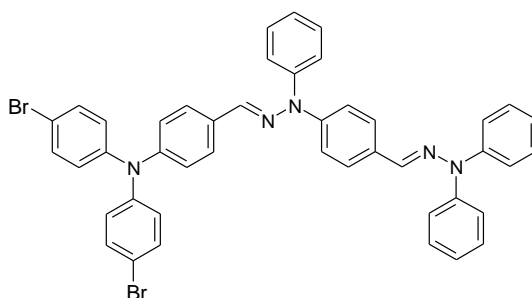
Synthesis of 4-bromo-*N*-(4-bromophenyl)-*N*-{4-[(2-{4-[(diphenylhydrazinylidene)methyl]phenyl}-2-phenylhydrazinylidene)methyl]phenyl}aniline (11): 2 g (2.83 mmol) of aldehyde **9** was dissolved in 25 mL of toluene, 1.25 g (5.66 mmol) of 1,1-diphenylhydrazine hydrochloride were extracted with toluene and a saturated water solution of K$_2$CO$_3$. The organic layer was added into the reaction mixture together with a catalytic

amount of acetic acid. The mixture was heated for 30 min at reflux after which the reaction was terminated and the solvent removed (TLC acetone/*n*-hexane = 1:24). The crude product was purified by column chromatography (0.5:24.5 v/v acetone/*n*-hexane) to give **11** as a yellow solid (2.011 g, 90%). ^{1}H NMR (700 MHz, CDCl$_3$, 25°C, TMS): 7.60 (d, J = 8.7 Hz, 2H), 7.50 – 7.44 (m, 4H), 7.41 (m, 4H), 7.34 (d, J = 8.8 Hz, 4H), 7.27 (t, J = 7.4 Hz, 1H), 7.25 (s, 1H), 7.21 – 7.16 (m, 7H), 7.16 (s, 1H), 7.13 (m, 3H), 7.00 (d, J = 8.7 Hz, 2H), 6.94 (d, J = 8.9 Hz, 4H) ppm; ^{13}C NMR (176 MHz, CDCl$_3$, 25°C, TMS): 146.97, 146.33, 144.62, 143.89, 142.50, 135.50, 135.44, 132.57, 131.49, 131.44, 130.25, 129.92, 127.67, 127.59, 125.91, 125.85, 124.69, 124.55, 124.12, 122.65, 120.53, 116.00 ppm;

Elemental analysis calcd (%) for C$_{44}$H$_{33}$N$_5$Br$_2$: C 66.76, H 4.20, N 8.85; found: C 66.65, H 4.08, N 8.91.

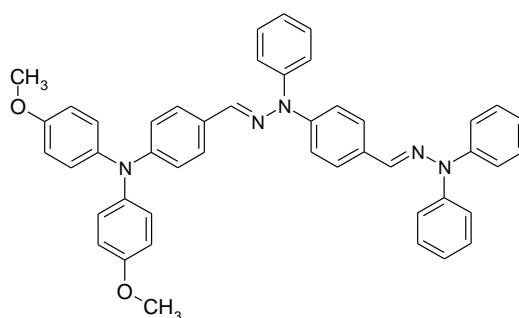**Synthesis of 4-methoxy-*N*-(4-methoxyphenyl)-*N*-{4-[(2-{4-[(2-methyl-2-phenylhydrazinylidene)methyl]phenyl}-2-phenylhydrazinylidene)methyl]phenyl}aniline (12):** 0.436 g (18.94 mmol) of sodium was dissolved in 5.5 mL of anhydrous methanol under argon atmosphere. 0.691 g (0.947 mmol) of hydrazone **10** were dissolved in 20 mL of anhydrous DMF and added into the sodium methoxide solution along with 0.757 g (3.977 mmol) of CuI. The mixture was heated at 100°C 5 h. After termination of the reaction, the mixture was extracted with ethyl acetate (TLC acetone/*n*-hexane = 2:23). The organic layer was dried over anhydrous Na$_2$SO$_4$, filtered and the solvent was removed. The crude product was purified by column chromatography (1.5:3:20.5 v/v ethyl acetate/toluene/*n*-hexane) to give **12** as a yellow solid (0.19 g, 32%). ^{1}H NMR (400 MHz, CDCl$_3$, 25°C, TMS) δ 7.71 (s, 1H), 7.68 (s, 1H), 7.51 (s, 1H), 7.48 – 7.34 (m, 5H), 7.34 – 7.27 (m, 2H), 7.26 – 7.19 (m, 4H), 7.16 (d, J = 8.5 Hz, 3H), 7.07 – 7.01 (m, 4H), 6.94 – 6.85 (m, 3H), 6.82 (d, J = 8.9 Hz, 4H), 3.79 (s, 6H), 3.43 (s, 3H) ppm; ^{13}C NMR (101 MHz, CDCl$_3$, 25°C, TMS): 156.07, 149.01, 148.05, 144.23, 143.04, 140.75, 136.45, 132.10, 131.85, 130.09, 129.15, 128.28, 127.40, 127.25, 126.79, 125.28, 124.16, 121.09, 120.46, 120.35, 115.22, 114.81, 55.62, 33.20 ppm;

Elemental analysis calcd (%) for C$_{41}$H$_{37}$N$_5$O$_2$: C 77.95, H 5.90, N 11.09; found: C 78.06, H 5.98, N 10.99.
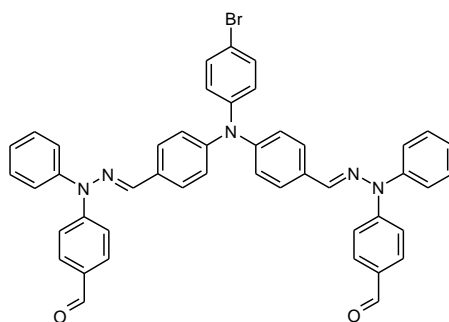
Synthesis of 4-[(2-{4-[(diphenylhydrazinylidene)methyl]phenyl}-2-phenylhydrazinylidene)methyl]-*N*,*N*-bis(4-methoxyphenyl)aniline (13): 1.52 g (65.9 mmol) of sodium was dissolved in 18 mL of anhydrous methanol under argon atmosphere . 2.011 (2.54 mmol) of hydrazone **11** were dissolved in 40 mL of anhydrous DMF and added into the sodium methoxide solution along with 1.901 g (10.017 mmol) of CuI. The mixture was heated at 100°C 15 h. After termination of the reaction, the mixture was extracted with ethyl acetate (TLC acetone/*n*-hexane = 2:23). The organic layer was dried over anhydrous Na_2SO_4, filtered, the solvent was removed. The crude product was purified by column chromatography (1:2:22 v/v ethyl acetate/toluene/*n*-hexane; DCM) to give **13** as a yellow solid (0.244 g, 14%). ^{1}H NMR (700 MHz, CDCl$_3$, 25°C, TMS): 7.58 (d, J = 8.7 Hz, 2H), 7.45 (t, J = 7.9 Hz, 2H), 7.41 (t, J = 8.0 Hz, 6H), 7.27 – 7.23 (m, 2H), 7.21 – 7.16 (m, 7H), 7.15 (s, 1H), 7.13 – 7.09 (m, 3H), 7.04 (d, J = 9.0 Hz, 4H), 6.87 (d, J = 8.8 Hz, 2H), 6.82 (d, J = 9.0 Hz, 4H), 3.79 (s, 6H) ppm; ^{13}C NMR (176 MHz, CDCl$_3$, 25°C, TMS): 156.14, 149.10, 145.02, 143.95, 142.65, 140.78, 136.63, 135.67, 131.03, 130.19, 129.90, 128.24, 127.62, 127.29, 126.83, 125.75, 124.91, 124.48, 122.65, 120.36, 120.30, 114.85, 55.64 ppm;

Elemental analysis calcd (%) for $C_{46}H_{39}N_5O_2$: C 79.63, H 5.76, N 10.09; found: C 79.68, H 5.71, N 10.24.
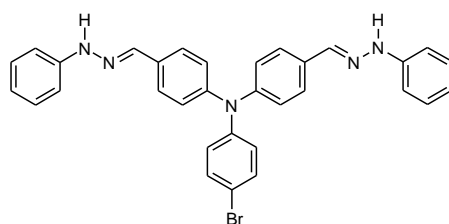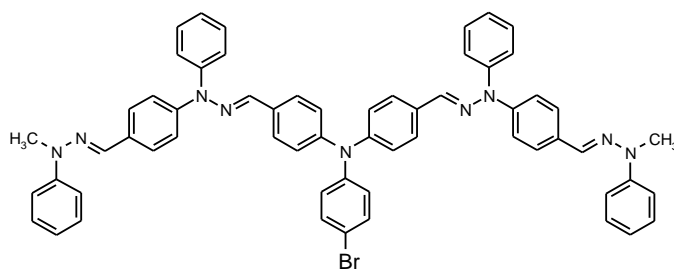

Synthesis of 4-bromo-*N*,*N*-bis{4-[(2-phenylhydrazinylidene)methyl]phenyl}aniline (14): 9.36 g (24.616 mmol) of 4.4'-diformyl-4''-bromotriphenylamine were dissolved in a mixture of THF and isopropanol (60 mL, 2:1, v/v). 7.53 mL (76.31 mmol) of phenylhydrazine were added to and the reaction was heated at 70°C for 1 h and cooled to RT (TLC acetone/*n*-hexane = 3:22). Formed crystals were filtered and washed with a mixture of *n*-hexane and isopropanol (1:1, v/v) to give **14** as yellow crystals (9.91 g, 71%). Hydrazone **14** was used in the next step without purification.

Synthesis of 4,4'-([(4-bromophenyl)imino]bis{benzene-4,1-diylmethylylidene[1-phenylhydrazin-1-yl-2-ylidene]})dibenzaldehyde (15): 9.91 g (17.68 mmol) of hydrazone **14**, 14.66 g (106.08 mmol) K_2CO_3 and 5.69 mL (53.042 mmol) *p*-fluorobenzaldehyde were dissolved in 100 mL of anhydrous DMF, under argon atmosphere. The mixture was heated for 4 h at reflux. After termination of the reaction, the mixture was extracted with ethyl acetate (TLC ethyl acetate/*n*-hexane = 5:20). The organic layer was dried over anhydrous Na_2SO_4, filtered, the solvent was removed. The crude product was purified by column chromatography (1:2:22 v/v acetone/THF/*n*-hexane) to give **15** as an orange amorphous mass (6.011 g, 48%). ^{1}H NMR (700 MHz, Acetone-d6, 25°C, TMS): 9.85 (s, 2H), 7.82 – 7.73 (m, 7H), 7.67 – 7.62 (m, 6H), 7.49 (d, J = 7.2 Hz, 2H), 7.36 (d, J = 8.0 Hz, 4H), 7.29 (s, 2H), 7.27 – 7.22 (m, 5H), 7.10 – 7.03 (m, 6H) ppm; ^{13}C NMR (176 MHz, Acetone-d6, 25°C, TMS) δ 190.92, 152.94, 148.63, 139.49, 139.33, 133.53, 132.31, 132.00, 131.65, 130.81, 130.59, 130.38, 129.91, 129.19, 129.06, 127.40, 124.96, 115.17 ppm;

Elemental analysis calcd (%) for $C_{46}H_{34}N_5BrO_2$: C 71.87, H 4.46, N 9.11; found: C 72.00, H 4.43, N 9.12.

Synthesis of 4-bromo-*N*-{4-[(2-{4-[(2-methyl-2-phenylhydrazinylidene)methyl]phenyl}-2-phenylhydrazinylidene)methyl]phenyl}-*N*-{4-[(2-{4-[(2-methyl-2-phenylhydrazinylidene)methyl]phenyl}-2-phenylhydrazinylidene)methyl]phenyl}aniline (16): 3 g (4.238 mmol) of substance **15** was dissolved in 25 mL of toluene, 1.3 mL (11.02 mmol) 1-phenyl-1-methylhydrazine and a catalytic amount of acetic acid were added. The mixture was heated for 1 h at reflux after which the reaction was terminated and the solvent removed. The crude product was purified by column chromatography (2:4:19 v/v ethyl acetate/toluene/*n*-hexane) to give **16** as a yellow solid (2.29 g,

55%). ^{1}H NMR (700 MHz, CDCl$_3$, 25°C, TMS): 7.71 (d, J = 8.5 Hz, 4H), 7.50 (m, 6H), 7.46 (t, J = 7.7 Hz, 4H), 7.39 – 7.29 (m, 10H), 7.26 – 7.20 (m, 7H), 7.19 – 7.15 (m, 5H), 7.03 (d, J = 8.6 Hz, 3H), 6.97 (d, J = 8.8 Hz, 3H), 6.92 (t, J = 6.8 Hz, 2H), 3.43 (s, 6H) ppm; ^{13}C NMR (CDCl$_3$, 176 MHz, 25°C, TMS): 148.07, 147.10, 143.96, 142.98, 135.56, 132.52, 132.47, 131.72, 131.31, 130.15, 129.17, 129.05, 127.52, 127.47, 126.17, 125.96, 125.46, 124.21, 124.03, 121.32, 120.57, 115.30, 33.24, 30.47 ppm;

Elemental analysis calcd (%) for C$_{60}$H$_{50}$N$_9$Br: C 73.76, H 5.16, N 12.90; found: C 73.63, H 5.21, N 12.99.
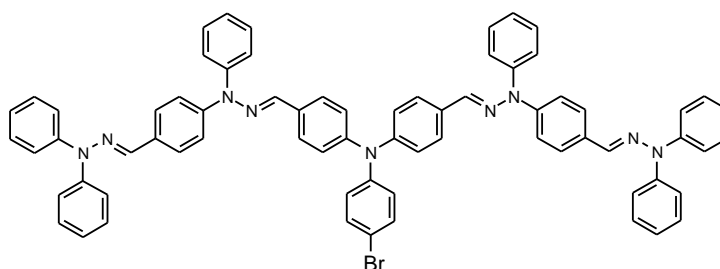
Synthesis of 4-bromo-*N*,*N*-bis{4-[(2-{4-[(diphenylhydrazinylidene)methyl]phenyl}-2-phenylhydrazinylidene)methyl]phenyl}aniline (17): 2.81 g (3.97 mmol) of aldehyde **15** was dissolved in 30 mL of toluene. 2.8925 g (13.102 mmol) of 1,1-diphenylhydrazine hydrochloride were extracted with toluene and a saturated water solution of K$_2$CO$_3$. The organic layer was added into the reaction mixture together with a catalytic amount of acetic acid. The mixture was heated for 30 min at reflux after which the reaction was terminated and the solvent removed. The crude product was purified by column chromatography (1:1:23 v/v ethyl acetate/toluene/*n*-hexane) to give **17** as a yellow solid (2.388 g, 59%). ^{1}H NMR (700 MHz, CDCl$_3$, 25°C, TMS): 7.60 (d, J = 8.2 Hz, 3H), 7.51 – 7.44 (m, 6H), 7.41 (t, J = 7.5 Hz, 6H), 7.34 (d, J = 8.1 Hz, 2H), 7.30 – 7.23 (m, 8H), 7.23 – 7.10 (m, 20H), 7.04 – 7.00 (m, 6H), 6.99 – 6.93 (m, 3H) ppm; ^{13}C NMR (176 MHz, CDCl$_3$, 25°C, TMS): 170.32, 149.35, 148.50, 147.12, 146.43, 144.69, 143.90, 142.50, 135.67, 135.48, 132.47, 131.42, 131.23, 130.24, 129.91, 129.19, 129.15, 127.66, 127.52, 125.98, 125.90, 124.74, 124.53, 124.18, 122.84, 122.65, 122.09, 121.22, 120.49, 119.61, 117.95, 115.84 ppm;

Elemental analysis calcd (%) for C$_{70}$H$_{54}$N$_5$Br: C 76.35, H 4.94, N 11.45; found: C 76.66, H 4.77, N 11.74.
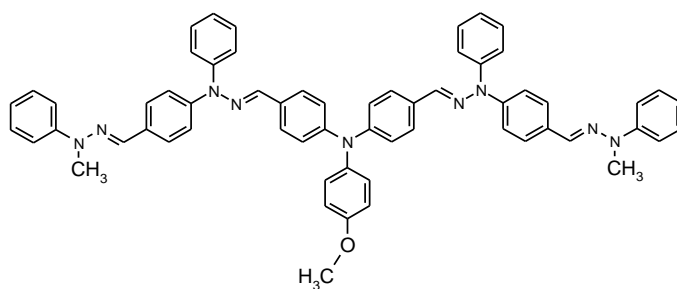
Synthesis of 4-methoxy-*N*-{4-[(2-{4-[(2-methyl-2-phenylhydrazinylidene)methyl]phenyl}-2-phenylhydrazinylidene)methyl]phenyl}-*N*-{4-[(2-{4-[(2-methyl-2-phenylhydrazinylidene)methyl]phenyl}-2-phenylhydrazinylidene)methyl]phenyl}aniline (18): 1.1 g (47.826 mmol) of sodium was dissolved in 15 mL of anhydrous methanol under argon atmosphere. 2.293 (2.54 mmol) of hydrazone **16** were dissolved in 18 mL of anhydrous DMF and the mixture was added into the sodium methoxide solution along with 0.98 g (5.14 mmol) of CuI. The mixture was heated at 100°C 4 h. After termination of the reaction, the mixture was extracted with ethyl acetate. The organic layer was dried over anhydrous Na_2SO_4, filtered, the solvent was removed. The crude product was purified by column chromatography (2:5:18 v/v toluene/THF/*n*-hexane) to give **18** as a yellow solid (0.515 g, 23%). ^{1}H NMR (700 MHz, CDCl$_3$, 25°C, TMS): 7.70 (d, *J* = 8.6 Hz, 4H), 7.51 (s, 2H), 7.48 − 7.42 (m, 7H), 7.37 (d, *J* = 8.6 Hz, 4H), 7.31 (dd, *J* = 8.4, 7.5 Hz, 4H), 7.26 − 7.20 (m, 6H), 7.19 − 7.13 (m, 7H), 7.06 (d, *J* = 8.9 Hz, 2H), 7.00 (d, *J* = 8.7 Hz, 4H), 6.91 (t, *J* = 6.9 Hz, 2H), 6.84 (d, *J* = 8.9 Hz, 2H), 3.80 (s, 3H), 3.42 (s, 6H) ppm; ^{13}C NMR (176 MHz, CDCl$_3$, 25°C, TMS): 156.55, 147.94, 147.76, 143.98, 142.89, 140.01, 137.87, 132.19, 131.66, 129.98, 129.89, 129.02, 127.51, 127.30, 127.21, 125.24, 123.97, 122.73, 121.07, 120.38, 115.14, 114.86, 55.49, 33.08 ppm;

Elemental analysis calcd (%) for $C_{61}H_{53}N_9O$: C 78.94, H 5.76, N 13.58; found: C 79.06, H 5.51, N 13.69.
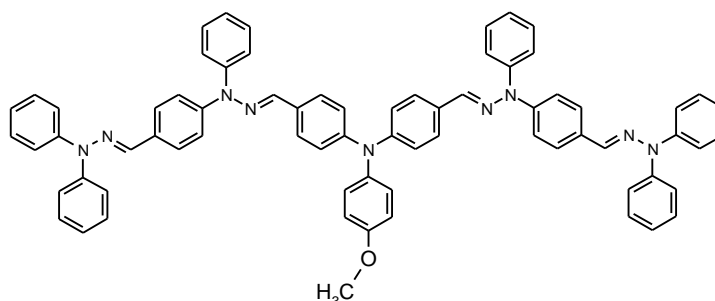
Synthesis of 4-[(2-{4-[(diphenylhydrazinylidene)methyl]phenyl}-2-phenylhydrazinylidene)methyl]-*N*-{4-[(2-{4-[(diphenylhydrazinylidene)methyl]phenyl}-2-phenylhydrazinylidene)methyl]phenyl}-*N*-(4-methoxyphenyl)aniline (19): 1 g (43.4783 mmol) of sodium was dissolved in 7 mL of anhydrous methanol under argon atmosphere. 1 g

(0.9868 mmol) of hydrazone **17** was dissolved in 10 mL of anhydrous DMF and the mixture was added into the sodium methoxide solution along with 0.395 g (2.0723 mmol) of CuI. The mixture was placed in a closed vessel into a microwave reactor and heated at 105°C (100W), for 1 h. After termination of the reaction, the mixture was extracted with ethyl acetate. The organic layer was dried over anhydrous Na_2SO_4, filtered, the solvent was removed. The crude product was purified by column chromatography (0.5:2:7.5 v/v ethyl acetate/toluene/*n*-hexane) to give **19** as a yellow solid (0.113 g, 11%). ^{1}H NMR (700 MHz, CDCl$_3$, 25°C, TMS): 7.59 (d, *J* = 8.7 Hz, 3H), 7.47 – 7.43 (m, 6H), 7.43 – 7.38 (m, 9H), 7.29 – 7.24 (m, 4H), 7.22 – 7.10 (m, 24H), 7.10 – 7.03 (m, 4H), 6.99 (d, *J* = 8.7 Hz, 3H), 6.84 (d, *J* = 9.0 Hz, 1H), 3.80 (s, 3H). ^{13}C NMR (176 MHz, CDCl$_3$, 25°C, TMS): 157.72, 156.71, 147.93, 144.85, 143.92, 143.87, 142.56, 140.11, 138.59, 136.14, 135.58, 134.14, 133.37, 133.32, 131.22, 130.26, 130.22, 129.96, 129.92, 129.90, 129.87, 129.52, 128.46, 127.72, 127.68, 127.66, 127.64, 127.36, 126.32, 125.84, 125.80, 125.20, 124.83, 124.61, 124.57, 124.50, 124.36, 122.85, 122.64, 120.61, 120.47, 120.38, 119.38, 118.48, 117.27, 115.38, 115.00, 114.89, 55.64 ppm;

Elemental analysis calcd (%) for $C_{71}H_{57}N_9O$: C 81.04, H 5.46, N 11.98; found: C 81.22, H 5.53, N 11.65.

5. Results and conclusions

1. New di- and tetrahydrazones with triphenylamine based central fragments have been synthesized.
2. The thermal, photoelectric and electrochemical properties of the synthesized materials have been explored and the following conclusions have been made:
   a) dihydrazones can form crystals as well as amorphous glass, whereas tetrahydrazones are fully amorphous;
   b) the structural disorder introduced by additional hydrazone fragments reduces the influence moieties at the end hydrazone fragments have on various properties;
   c) the introduction of electron-donoric methoxy moieties reduced ionization potential and oxidation energy across the board, allowing to reach values as low as 5,1 eV and 0.74 V, which are comparable with those of 2,2',7,7'-tetrakis-(*N*,*N*-di-4-methoxyphenylamino)-9,9'-spirobifluorene (5.00 eV and 0.69 V accordingly);
   d) methoxy moieties also influence molecular packing in such a way that hole drift mobilities as high as 2.5×10^{-3} cm^2 V^{-1}s^{-1} could be achieved in tetrahydrazones **18**, **19** which is an order of magnitude higher than that of 2,2',7,7'-tetrakis-(*N*,*N*-di-4-methoxyphenylamino)-9,9'-spirobifluorene.
3. During the preliminary solar cell tests the hydrazones demonstrated power conversion efficiencies as high as 1.6% in solid state dye-sensitized solar cells and 1.1% in perovskite solar cells. Judging from the test results the doping procedures used for 2,2',7,7'-tetrakis-(*N*,*N*-di-4-methoxyphenylamino)-9,9'-spirobifluorene are not suitable for these materials. It is hypothesized that higher ionization potential of the investigated hydrazones hinders the doping process and the conductivity remains low, which is confirmed by rather low fill factors. Further optimization of the doping procedure and device construction is necessary in order to enhance the performance of hydrazones as hole transporting materials in solar cells.

List of publications

1. **A. Kolesničenko**, T. Malinauskas, "Di- ir tetrahidrazono fragmentus turinčių metoksitrifenilamino darinių sintezė" // Conference presentation materials from "Chemistry and chemical technology 2014"; Kaunas, 2014, p. 9-10.

2. **Aleksandras Kolesnicenko**, Tadas Malinauskas, Ernestas Kasparavicius, Robert Send, Valentas Gaidelis, Vygintas Jankauskas, Henrike Wonneberger, Ingmar Bruder, Vytautas Getautis, Investigation of a dendrimer-like arrangement of hydrazone fragments for the application as hole transporting materials // Submitted to Tetrahedron

Acknowledgments

References

1. Hammarström L., Hammes-Schiffer S. Artificial Photosynthesis and Solar Fuels. Accounts of Chemical Research, 2009, vol. 42, p. 1859-2029.

2. Lygaitis R., Getautis V., Gražulevičius J. V., Hole-transporting Hydrazones. Chemical Society Reviews, 2008, vol. 37, p. 770-788.

3. Zhang W., Cheng Y., Ying X., Liu B. Solid-State Dye-Sensitized Solar Cells with Conjugated Polymers as Hole-Transporting Materials. Macromolecular Chemistry and Physics, 2011, vol. 212, p. 15-23.

4. Kim H-S., Lee C-R., Im J-H., Lee K-B., Moehl R., Marchioro A., Moon S-J., Humphry-Baker R., Yum J-H., Moser J. E., Grätzel M., Park N-G. Lead Iodide Perovskite Sensitized All-Solid-State Submicron Thin Film Mesoscopic Solar Cell with Efficiency Exceeding 9%. Scientific Reports, 2012, vol. 2, p. 591.

5. Lee M. M., Teuscher J., Miyasaka T., Murakami T. N., Snaith H. J. Efficient Hybrid Solar Cells Based on Meso-Superstructured Organometal Halide Perovskites. Science, 2012, vol. 338, p. 643-647.

6. *Melas-Kyriazi* J., Ding I-K., Marchioro A., Punzi A., Hardin B. E., Burkhard G. F., Tetrault G. F., Tetrault N., *Grätzel* M., Moser J-E., McGehee M. D. The Effect of Hole Transport Material Pore Filling on Photovoltaic Performance in Solid-State Dye-Sensitized Solar Cells. Advanced Energy Materials, 2011, vol. 1, p. 407-414.

7. H.O. Wirth // *Angew. Makromol. Chem*, 1991, 185-186 p.

8. Coropceanu V., Cornil J., da Silva Filho D. A., Olivier Y., Silbey R., Brédas J. L. Charge transport in organic semiconductors. Chemical Reviews, 2007, vol 107 (4), p. 926-952.

9. Nomura S., Shirota Y. Concentration dependence of the activation energy for the hole drift mobility of 9-ethylcarbazole-3-carbaldehyde diphenylhydrazone dispersed in polycarbonate. Chemical Physics Letters, 1997, vol. 268, p. 461-464.

10. Yu Z., Sun L. Recent Progress on Hole-Transporting Materials for Emerging Organometal Halide Perovskite Solar Cells. In: Advanced Energy Materials, ed. J. Ritterbusch [online]. Wiley Online Library [first published 2015.04.20]. Available from: http://onlinelibrary.wiley.com/doi/10.1002/aenm.201500213.

11. Miyamoto E., Yamaguchi Y., Masaaki M. Electrophotography, 1989, vol. 28, p. 364.

12. Ooyama Y., Harima Y. Molecular Designs and Syntheses of Organic Dyes for Dye-Sensitized Solar Cells. The Journal of Organic Chemistry, 2009, vol. 18, p. 2903–2934.

13. Bach U., Lupo D., Comte P., Moser J. E., Weissörtel F., Salbeck J., Spreitzer H., Grätzel M. Solid-state Dye-sensitized Mesoporous TiO$_2$ Solar Cells With High Photon-to-electron Conversion Efficiencies. Nature, 1998, vol. 395, p. 583-585.

14. Liu M., Johnston M. B., Snaith H. J. Efficient planar heterojunction perovskite solar cells by vapour deposition. Nature, 2013, vol. 501, p. 395-398.

15. Huang F., Dkhissi Y., Huang W., Xiao N., Benesperi I., Rubanov S., Zhu Y., Lin X., Jiang L., Zhou Y., Gray-Weale A., Etheridge J., McNeill C. R., Caruso R. A., Bach U., Spicca L., Cheng Y-B. Gas-assisted preparation of lead iodide perovskite films consisting of a monolayer of single crystalline grains for high efficiency planar solar cells. Nano Energy, 2014, vol. 10, p. 10-18.

16. Zhou H., Chen Q., Li G., Luo S., Song T-B., Duan H-S., Hong Z., You J., Liu Y., Yang Y. Interface engineering of highly efficient perovskite solar cells. Science, 2014, vol. 345, p. 542-546.

17. Jeon N. J., Lee H. G., Kim Y. C., Seo J., Noh J. H., Lee J. Seok S. I. o-Methoxy Substituents in Spiro-OMeTAD for Efficient Inorganic−Organic Hybrid Perovskite Solar Cells. Journal of the American Chemical Society, 2014, vol. 136, p. 7837-7840.

18. Burschka J., Dualeh A., Kessler F., Baranoff E., Cevey-Ha N-L., Yi C., Nazeeruddin M. K., Gr€atzel M. Tris(2-(1H-pyrazol-1-yl)pyridine)cobalt(III) as p-Type Dopant for Organic Semiconductors and Its Application in Highly Efficient Solid-State Dye-Sensitized Solar Cells. Journal of the American Chemical Society, 2011, vol. 133, p. 18042-18045.

19. Abate A., Hollman D. J., Teuscher J., Pathak S., Avolio R., D'Errico G., Vitiello G., Fantacci S., Snaith H. J. Protic Ionic Liquids as p‑Dopant for Organic Hole Transporting Materials and Their Application in High Efficiency Hybrid Solar Cells. Journal of the American Chemical Society, 2013, vol. 135, p. 13538-13548.

20. Nguyen W. H., Bailie C. D., Unger E. L., McGehee M. D. Enhancing the Hole-Conductivity of Spiro-OMeTAD without Oxygen or Lithium Salts by Using Spiro(TFSI)2 in Perovskite and Dye-Sensitized Solar Cells. Journal of the American Chemical Society, 2014, vol. 136, p. 10996-11001.

21. Zheng. L., Chung Y-H., Ma L. Z., Xiao L., Chen Z., Wang S., Qu B., Gong Q. A hydrophobic hole transporting oligothiophene for planar perovskite solar cells with improved stability. Chemical Communications, 2014, vol. 50, p. 11196-11199.

22. Liu J., Wu Y., Qin C., Yang X., Yasuda T., Islam A., Zhang K., Peng W., Chen W., Han L. A dopant-free hole-transporting material for efficient and stable perovskite solar cells. Energy & Environmental Science, 2014, vol. 7, p. 2963-2967.

23. Hawash Z., Ono L. K., Raga S. R., Lee M. V., Qi Y. Air-Exposure Induced Dopant Redistribution and Energy Level Shifts in Spin-Coated Spiro-MeOTAD Films. Chemistry of Materials, 2015, vol. 27 (2), p. 562-569.

24. Jeon N. J., Lee J., Noh J. H., Nazeeruddin M. K., Grätzel M., Seok S. I. Efficient Inorganic–Organic Hybrid Perovskite Solar Cells Based on Pyrene Arylamine Derivatives as Hole-Transporting Materials. Journal of the American Chemical Society, 2013, vol. 135 (51), p. 19087-19090.

25. Li. D. H., Fu K., Hafgeldt A., Grätzel M., Mhaisalkar S. G., Grimsdale A. C. A Simple 3,4-Ethylenedioxythiophene Based Hole-Transporting Material for Perovskite Solar Cells. Angewandte Chemie, 2014, vol. 53 (16), p. 4085-4088.

26. Li H., Fu K., Boix P. P., Wong L. H., Hagfeldt A., Grätzel M., Mhaisalkar S. G., Gimsdale A. C. Hole-Transporting Small Molecules Based on Thiophene Cores for High Efficiency Perovskite Solar Cells. ChemSusChem, 2014, vol. 7 (12), p. 3420-3425.

27. Krishna A., Sabba D., Li H., Yin J., Boix P. P., Soci C., Mhaisalkar S. G., Grimsdale A. C. Novel hole transporting materials based on triptycene core for high efficiency mesoscopic perovskite solar cells. Chemical Science, 2014, vol. 5, p. 2702-2709.

28. Do. K., Choi H., Lim K., Jo H., Cho J. W., Nazeeruddin M. K., Ko J. Star-shaped hole transporting materials with a triazine unit for efficient perovskite solar cells. Chemical Communications, 2014, vol. 50, p. 10971-10974.

29. Choi H., Paek S., Lim N., Lee Y. H., Nazeeruddin M. K., Ko J. Efficient Perovskite Solar Cells with 13.63 % Efficiency Based on Planar Triphenylamine Hole Conductors. Chemistry – A European Journal, 2014, vol. 20 (35), p. 10894-10899.

30. Sung S. D., Kang M. S., Choi I. T., Kim H. M., Kim H., Hong M-P., Kim H. K., Lee W. I. 14.8% perovskite solar cells employing carbazole derivatives as hole transporting materials. Chemical Communications, 2014, vol. 50, p. 14161-14163.

31. Qin P., Kast H., Nazeeruddin M. K., Zakeeruddin S. M., Mishra A., Bäuerle P., Grätzel M. Low band gap S,N-heteroacene-based oligothiophenes as hole-transporting and light absorbing materials for efficient perovskite-based solar cells. Energy & Environmental Science, 2014, vol. 7, p. 2981-2985.

32. Bi D., Yang L., Boschloo G., Hagfeldt A., Johansson E. M. J. Effect of Different Hole Transport Materials on Recombination in CH3NH3PbI3 Perovskite-Sensitized Mesoscopic Solar Cells. The Journal of Physical Chemistry, 2013, vol. 4 (9), p. 1532-1536.

33. Abrusci A., Stranks S. D., Docampo P., Yip H-L., Jen A. K-Y., Snaith H. J. High-Performance Perovskite-Polymer Hybrid Solar Cells via Electronic Coupling with Fullerene Monolayers. Nano Letters, 2013, vol. 13 (7), p. 3124-3128.

34. Kwon Y. S., Lim J., Yun H-J., Kim Y-H., Park T. A diketopyrrolopyrrole-containing hole transporting conjugated polymer for use in efficient stable organic–inorganic hybrid solar cells based on a perovskite. Energy & Environmental Science, 2014, vol. 7, p. 1454-1460.

35. Jeon N. J., Noh J. H., Yang W. S., Kim Y. C., Ryu S., Seo J., Seok S. I. Compositional engineering of perovskite materials for high-performance solar cells. Nature, 2015, vol. 517, p. 476-480.

36. Ryu S., Noh J. H., Jeon N. J., Kim Y. C., Yang W. S., Seo J., Seok S. I. Voltage output of efficient perovskite solar cells with high open-circuit voltage and fill factor. Energy & Environmental Science, 2014, vol. 7, p. 2614-2618.

37. Zhu Z., Bai Y., Ka H., Lee H., Mu C., Zhang T., Zhang L., Wang J., Yan H., So S. K., Yang S. Polyfluorene Derivatives are High-Performance Organic Hole-Transporting Materials for Inorganic−Organic Hybrid Perovskite Solar Cells. Advanced Functional Materials, 2014, vol. 24 (46), p. 7357-7365.

38. Y. P. Kitaev, B. I. M. Buzykin // *Hydrazony*, Nauka, Moskva, 1974, p. 21

39. Juozapavicius M., O'Regan B. C., Anderson A. Y., Grazulevicius J. V., Mimaite V. Efficient dye regeneration in solid-state dye-sensitized solar cells fabricated with melt processed hole conductors. Organic Electronics, 2012, vol. 13 (1), p. 23-30.

40. Shirota Y., Kageyama H. Charge Carrier Transporting Molecular Materials and Their Applications in Devices. Chemical Review, 2007, vol. 107, p. 953-1010.

41. Zhao Y., Ye C., Qiao Y., Xub W., Song Y., Zhu D. A novel donoreacceptor molecule containing a cyclic triphenylamine dimer: synthesis, characterization, and application in memory device. Tetrahedron, 2012, vol. 68, p. 1547-1551.